

A Kernel-Free Boundary Integral Method for Variable Coefficients Elliptic PDEs

Wenjun Ying^{1,*} and Wei-Cheng Wang²

¹ *Department of Mathematics, MOE-LSC and Institute of Natural Sciences, Shanghai Jiao Tong University, Minhang, Shanghai 200240, P.R. China.*

² *Department of Mathematics, National Tsing Hua University, and National Center for Theoretical Sciences, HsinChu, 300, Taiwan.*

Received 17 March 2013; Accepted (in revised version) 7 November 2013

Available online 21 January 2014

Abstract. This work proposes a generalized boundary integral method for variable coefficients elliptic partial differential equations (PDEs), including both boundary value and interface problems. The method is kernel-free in the sense that there is no need to know analytical expressions for kernels of the boundary and volume integrals in the solution of boundary integral equations. Evaluation of a boundary or volume integral is replaced with interpolation of a Cartesian grid based solution, which satisfies an equivalent discrete interface problem, while the interface problem is solved by a fast solver in the Cartesian grid. The computational work involved with the generalized boundary integral method is essentially linearly proportional to the number of grid nodes in the domain. This paper gives implementation details for a second-order version of the kernel-free boundary integral method in two space dimensions and presents numerical experiments to demonstrate the efficiency and accuracy of the method for both boundary value and interface problems. The interface problems demonstrated include those with piecewise constant and large-ratio coefficients and the heterogeneous interface problem, where the elliptic PDEs on two sides of the interface are of different types.

AMS subject classifications: 35J05, 65N06, 65N38

Key words: Elliptic partial differential equation, variable coefficients, kernel-free boundary integral method, finite difference method, geometric multigrid iteration.

1 Introduction

Variable coefficients elliptic partial differential equations (PDEs) appear in many important scientific and engineering applications such as the bidomain equations in compu-

*Corresponding author. *Email addresses:* wying@sjtu.edu.cn (W.-J. Ying), wangwc@math.nthu.edu.tw (W.-C. Wang)

tational cardiology [19, 30, 45], the Cahn-Hilliard equation [7, 15, 52] and the Poisson-Boltzmann equation [32, 50] in biophysics. Their accurate and efficient numerical method has long been an active research topic in computational physics [6, 10, 13, 16, 18, 20–22, 24, 25, 35, 36, 44].

Among the numerical methods developed for variable coefficients elliptic partial differential equations (PDEs), those working with Cartesian grids have their advantages in grid generation as well as algorithm efficiency and solution accuracy, and are often regarded to be more suitable for free boundary and moving interface problems than others, which are based on unstructured grids.

In this paper, we propose a new Cartesian grid based boundary integral method for both boundary value and interface problems of variable coefficients elliptic partial differential equation (PDE). The solution to the boundary value problem is computed by iteratively solving corresponding interface problems. The elliptic interface problem of our interest consists of the PDEs (2.5)-(2.6), the interface conditions (2.7) and the boundary condition (2.8) on the boundary of a rectangle. The PDEs (2.5)-(2.6) in the interface problem may be heterogeneous in the sense that the Green functions associated with the elliptic operators on two sides of the interface are in general different. For this, we call the interface problem (2.5)-(2.8) as a heterogeneous interface problem.

When the coefficients of the PDE are piecewise constant, the interface problem (2.5)-(2.8) can be solved by a fast Fourier transform (FFT) based iterative method [26]. Here we remark that the approach in [26] can only solve the special piecewise constant interface problem where the reaction coefficients simultaneously vanish or the ratio of them equals that of the diffusion coefficients. When the boundary condition (2.8) is further replaced by a far field boundary condition in the free space, the piecewise constant coefficients interface problem can be formulated as a boundary integral equation (BIE) and solved by a boundary integral method [47]. The standard boundary integral method requires an analytic expression of the kernel and the corresponding Green function. In general, for variable coefficients elliptic PDE, it is difficult if not impossible to find an analytical expression for the Green function. Even for constant coefficients elliptic PDE, if it is defined on a bounded domain and subject to a non-periodic boundary condition, the Green function is usually difficult to find, too. For this reason, the standard boundary integral method is traditionally restricted to the constant coefficients elliptic boundary value problem or the piecewise constant coefficients interface problem in a rectangle domain subject to the periodic boundary condition or in the free space subject to the far field radiation condition.

Other related works using Cartesian grid based methods include ones for boundary value problems [3, 4, 8, 11, 12, 17, 23, 31, 33, 34, 40] and those for interface problems [9, 25, 27–29, 37–39, 41, 46, 51]. All these methods are based on standard finite difference or finite element discretization. Near the boundary or interface, the discretization has to be modified in order to maintain desired accuracy. Most of the methods modify the coefficient matrix of the discrete linear system, which often makes it difficult to directly apply the geometric multigrid or FFT based fast solver. They have to resort to algebraic

multigrid (AMG) as the linear solver, whose performance depends closely on the matrix properties. We note that the approach in [11] leads to symmetric positive definite matrices for Dirichlet boundary value problems. The method in [29] adopts finite element formulation, with tailored basis functions near the interface, therefore also gives rise to a symmetric positive definite matrix. The method in [27] produces an M -matrix for interface problems. Some of the methods, such as [1], can be solved using a geometric multigrid type method. However, due to the coefficients discontinuity of the differential operator across the interface, efficient implementation of a geometric multigrid type method is far from trivial and may involve sophisticated construction of restricting and interpolating operations near the interface [1].

The kernel-free boundary integral (KFBI) method was originally proposed by Ying and Henriquez for elliptic boundary value problems [48, 49] as a generalization of the boundary integral method, particularly the grid-based boundary integral method by Mayo [33, 34]. The novelty of the KFBI method is to re-interpret all the boundary and volume integrals encountered as solutions to corresponding equivalent interface problems. For constant coefficients PDEs, the KFBI method is similar to the approach in [26]. In [48], the accuracy and efficiency of the KFBI method are demonstrated through numerical examples for constant coefficients elliptic PDEs, where one can solve the equivalent interface problem using fast Fourier transform.

This work is a further development of [48, 49] to variable coefficients boundary value and interface problems. One of the new ingredients here is the generalization of the classical boundary integral formulation to the heterogeneous interface problem. The corresponding boundary integral equations can be solved iteratively using a Krylov subspace method such as the generalized minimal residual (GMRES) method [42, 43]. Within each iteration, two much simpler interface problems are solved using a geometric multigrid preconditioned conjugate gradient (GMG-PCG) method.

We have conducted extensive numerical tests and found that both the numbers of GMG-PCG and GMRES iterations are independent of mesh size on all test problems. The computational cost by the method is essentially proportional to the number of unknowns. While this property is shared by most of the methods mentioned above, the advantage of the current approach is its simplicity in implementation. For the simpler interface problem whose solution is equivalent to evaluation of the corresponding boundary or volume integral, the coefficients of the elliptic operator are smooth across the interface. Therefore GMG-PCG can be easily implemented and work very efficiently with standard interpolating and restricting operators on Cartesian grids. In case the interface/boundary or the coefficients are time dependent, the overhead in updating the solver for the method is minimal compared to AMG or the method in [1]. This is easily seen by noting that the discretization is standard and uniform. No modification on the coefficient matrix of the resulting discrete system is required. The only correction involved near the interface is the source term.

The remainder of the paper is organized as follows. Section 2 describes the boundary value and interface problems of the variable coefficients elliptic PDEs. Section 3 reformu-

lates the boundary value and interface problems as boundary integral equations. Section 4 gives implementation details for a second-order version of the kernel-free boundary integral method in two space dimensions. Section 5 summarizes the KFBI method for the boundary value and interface problems. Numerical results demonstrating the efficiency and accuracy of the KFBI method are presented in Section 6. Finally, the KFBI method for the variable coefficients elliptic PDEs is summarized in Section 7. Limitation, extension and potential applications of the KFBI method for the variable coefficients elliptic PDEs are also discussed in the last section.

2 Variable coefficients elliptic PDEs

2.1 Boundary value problem

Let $\Omega_i \subset \mathbb{R}^d$ ($d=2$ or 3) be a bounded domain with smooth boundary $\Gamma = \partial\Omega_i$, which is in general irregular and complex (see Fig. 1). Let $\mathbf{p} \in \mathbb{R}^d$ be the space variable; $\sigma_i = \sigma_i(\mathbf{p}) \geq \sigma_0 > 0$ and $\kappa_i = \kappa_i(\mathbf{p}) \geq 0$ be the spatially variable smooth diffusion and reaction coefficients, respectively. Let $f_i = f_i(\mathbf{p})$ be a smooth function defined in Ω_i , too. Let $u = u(\mathbf{p})$ be the unknown function. We are interested in the numerical solution of both the Dirichlet boundary value problem

$$\mathcal{A}_i u \equiv \nabla \cdot (\sigma_i(\mathbf{p}) \nabla u) - \kappa_i(\mathbf{p}) u = f_i(\mathbf{p}) \quad \text{in } \Omega_i, \quad (2.1)$$

$$u = g^D \quad \text{on } \Gamma \equiv \partial\Omega_i, \quad (2.2)$$

and the Neumann boundary value problem

$$\mathcal{A}_i u = \nabla \cdot (\sigma_i(\mathbf{p}) \nabla u) - \kappa_i(\mathbf{p}) u = f_i(\mathbf{p}) \quad \text{in } \Omega_i, \quad (2.3)$$

$$\sigma_i \partial_{\mathbf{n}} u = g^N \quad \text{on } \Gamma, \quad (2.4)$$

for the variable coefficients elliptic partial differential equation (PDE). Here, \mathcal{A}_i is the differential operator of the elliptic PDE; g^D and g^N are, respectively, the Dirichlet and Neumann boundary data; \mathbf{n} denotes the unit outward normal vector on Γ and $\partial_{\mathbf{n}} u$ denotes the normal derivative of u .

2.2 Interface problem

Let $\mathcal{B} \subset \mathbb{R}^d$ ($d=2$ or 3) be a rectangle, and $\Gamma \subset \mathcal{B}$ be a smooth interface in \mathcal{B} , which separates the rectangle \mathcal{B} into two subdomains Ω_i and Ω_e , satisfying $\Gamma = \bar{\Omega}_i \cap \bar{\Omega}_e$ and $\Omega_i \cup \Gamma \cup \Omega_e = \mathcal{B}$. Assume that $\partial\Omega_i \cap \partial\mathcal{B} = \emptyset$ and $\partial\mathcal{B} \subset \partial\Omega_e$. By the assumptions, we have $\Gamma = \partial\Omega_i$. See Fig. 1 for an illustration. Let $\sigma_{i,0}$ and $\sigma_{e,0}$ be two positive constants; $\sigma_i \geq \sigma_{i,0}$, $\sigma_e \geq \sigma_{e,0}$, $\kappa_i \geq 0$, $\kappa_e \geq 0$, f_i and f_e be smooth functions defined on $\bar{\mathcal{B}}$. Assume that $\sigma_i(\mathbf{p})$ and $\sigma_e(\mathbf{p})$ are continuously differentiable on $\bar{\mathcal{B}}$ while noting that only the restriction of σ_i (σ_e) on



Figure 1: Irregular domain in a rectangle box.

Ω_i (Ω_e) appears in the original equation. Let $u_i = u_i(\mathbf{p})$ and $u_e = u_e(\mathbf{p})$ be the unknown functions. We consider the interface problem

$$\mathcal{A}_i u_i \equiv \nabla \cdot (\sigma_i(\mathbf{p}) \nabla u_i) - \kappa_i(\mathbf{p}) u_i = f_i(\mathbf{p}) \quad \text{in } \Omega_i, \tag{2.5}$$

$$\mathcal{A}_e u_e \equiv \nabla \cdot (\sigma_e(\mathbf{p}) \nabla u_e) - \kappa_e(\mathbf{p}) u_e = f_e(\mathbf{p}) \quad \text{in } \Omega_e, \tag{2.6}$$

subject to two interface conditions

$$u_i - u_e = g \quad \text{and} \quad \sigma_i \partial_{\mathbf{n}} u_i - \sigma_e \partial_{\mathbf{n}} u_e = j \quad \text{on } \Gamma, \tag{2.7}$$

and the boundary condition

$$u_e = 0 \quad \text{on } \partial \mathcal{B}. \tag{2.8}$$

Here, \mathcal{A}_i and \mathcal{A}_e are the differential operators for the elliptic PDEs in subdomains Ω_i and Ω_e , respectively; \mathbf{n} represents the unit normal vector pointing from Ω_i to Ω_e on the interface Γ . Typical examples of the interface problem arise from the temporally implicit semi-discrete discretization of the Stefan problem and the linearization of the Poisson-Boltzmann equation.

3 The boundary integral formulations

The boundary value and interface problems described in the previous section are reformulated as boundary integral equations in this section.

3.1 Boundary value problem

Let $\mathcal{B} \subset \mathbb{R}^d$ be a larger rectangle (see Fig. 1), which embeds domain Ω_i for the boundary value problems (2.1)-(2.2) and (2.3)-(2.4).

Assume $\sigma_i(\mathbf{p})$ is continuously differentiable and $\kappa_i(\mathbf{p})$ is continuous on $\bar{\mathcal{B}}$ even though only their restrictions on Ω_i appear in the PDE. Let $G_i(\mathbf{p}, \mathbf{q})$ be the Green function associated with the variable coefficients elliptic PDE on the rectangle \mathcal{B} , which satisfies

$$\begin{aligned} \mathcal{A}_i G_i(\mathbf{p}, \mathbf{q}) &= \nabla_{\mathbf{p}} \cdot (\sigma_i(\mathbf{p}) \nabla_{\mathbf{p}} G_i(\mathbf{p}, \mathbf{q})) - \kappa_i(\mathbf{p}) G_i(\mathbf{p}, \mathbf{q}) = \delta(\mathbf{p} - \mathbf{q}) && \text{in } \mathcal{B}, \\ G_i(\mathbf{p}, \mathbf{q}) &= 0 && \text{on } \partial \mathcal{B}. \end{aligned}$$

Here, $\delta(\mathbf{p}-\mathbf{q})$ is the Dirac delta function; $\nabla_{\mathbf{p}}$ stands for the gradient operator with respect to the space variable $\mathbf{p} \in \mathbb{R}^d$.

Let $H^{1/2}(\Gamma)$ be the trace space of Sobolev space $H^1(\Omega_i)$ on $\Gamma = \partial\Omega_i$ and $H^{-1/2}(\Gamma)$ be the dual space of $H^{1/2}(\Gamma)$. Let $\mathbf{n}_{\mathbf{p}}$ be the unit outward normal vector at point $\mathbf{p} \in \Gamma$. For density function $\varphi \in H^{1/2}(\Gamma)$, define the double layer boundary integral by

$$\begin{aligned} \mathcal{M}_i\varphi(\mathbf{p}) &\equiv \int_{\Gamma} \sigma_i(\mathbf{q}) \frac{\partial G_i(\mathbf{q}, \mathbf{p})}{\partial \mathbf{n}_{\mathbf{q}}} \varphi(\mathbf{q}) ds_{\mathbf{q}} \\ &= \int_{\Gamma} \sigma_i(\mathbf{q}) \mathbf{n}_{\mathbf{q}} \cdot \nabla_{\mathbf{q}} G_i(\mathbf{q}, \mathbf{p}) \varphi(\mathbf{q}) ds_{\mathbf{q}} \in H^{1/2}(\Gamma) \end{aligned}$$

and the hyper-singular boundary integral by

$$\begin{aligned} \mathcal{N}_i\varphi(\mathbf{p}) &\equiv \int_{\Gamma} \sigma_i(\mathbf{p}) \sigma_i(\mathbf{q}) \frac{\partial^2 G_i(\mathbf{q}, \mathbf{p})}{\partial \mathbf{n}_{\mathbf{p}} \partial \mathbf{n}_{\mathbf{q}}} \varphi(\mathbf{q}) ds_{\mathbf{q}} \\ &= \int_{\Gamma} \sigma_i(\mathbf{p}) \sigma_i(\mathbf{q}) \mathbf{n}_{\mathbf{p}}^T (\nabla_{\mathbf{p}} \nabla_{\mathbf{q}} G_i(\mathbf{q}, \mathbf{p})) \mathbf{n}_{\mathbf{q}} \varphi(\mathbf{q}) ds_{\mathbf{q}} \in H^{-1/2}(\Gamma). \end{aligned}$$

For density function $\psi \in H^{-1/2}(\Gamma)$, define the single layer boundary integral by

$$\mathcal{L}_i\psi(\mathbf{p}) \equiv \int_{\Gamma} G_i(\mathbf{q}, \mathbf{p}) \psi(\mathbf{q}) ds_{\mathbf{q}} \in H^{1/2}(\Gamma)$$

and the adjoint double layer boundary integral by

$$\begin{aligned} \mathcal{M}_i^*\psi(\mathbf{p}) &\equiv \int_{\Gamma} \sigma_i(\mathbf{p}) \frac{\partial G_i(\mathbf{q}, \mathbf{p})}{\partial \mathbf{n}_{\mathbf{p}}} \psi(\mathbf{q}) ds_{\mathbf{q}} \\ &= \int_{\Gamma} \sigma_i(\mathbf{p}) \mathbf{n}_{\mathbf{p}} \cdot \nabla_{\mathbf{p}} G_i(\mathbf{q}, \mathbf{p}) \psi(\mathbf{q}) ds_{\mathbf{q}} \in H^{-1/2}(\Gamma). \end{aligned}$$

Define the volume integral on Ω_i by

$$\mathcal{G}_i f_i(\mathbf{p}) \equiv \int_{\Omega_i} G_i(\mathbf{q}, \mathbf{p}) f_i(\mathbf{q}) d\mathbf{q}.$$

In terms of the Green function, the Dirichlet BVP (2.1)-(2.2) can be reformulated as a Fredholm boundary integral equation of the second kind,

$$\frac{1}{2}\varphi(\mathbf{p}) + \mathcal{M}_i\varphi(\mathbf{p}) = g^D(\mathbf{p}) - \mathcal{G}_i f_i(\mathbf{p}) \quad \text{for } \mathbf{p} \in \Gamma. \tag{3.1}$$

The solution to the Dirichlet BVP reads

$$u(\mathbf{p}) = \mathcal{M}_i\varphi(\mathbf{p}) + \mathcal{G}_i f_i(\mathbf{p}) \quad \text{for } \mathbf{p} \in \Omega. \tag{3.2}$$

The Neumann BVP (2.3)-(2.4) can be reformulated as a Fredholm boundary integral equation of the second kind,

$$\frac{1}{2}\psi(\mathbf{p}) - \mathcal{M}_i^*\psi(\mathbf{p}) = g^N(\mathbf{p}) - \mathbf{n}_{\mathbf{p}} \cdot \sigma_i(\mathbf{p}) \nabla_{\mathbf{p}} \mathcal{G}_i f_i(\mathbf{p}) \quad \text{for } \mathbf{p} \in \Omega. \tag{3.3}$$

The solution to the Neumann BVP reads

$$u(\mathbf{p}) = -\mathcal{L}_i\psi(\mathbf{p}) + \mathcal{G}_i f_i(\mathbf{p}) \quad \text{for } \mathbf{p} \in \Omega. \tag{3.4}$$

Remark 3.1. The BIE (3.1) or (3.3) for the corresponding BVP can be derived by potential decomposition together with the continuity property of the volume integral $\mathcal{G}_i f_i$ and the jump relations that the double layer potential $\mathcal{M}_i \varphi$ and the normal derivative of the single layer potential $\mathcal{L}_i \psi$ satisfy. See Theorems A.1-A.3 in the appendix for the continuity and discontinuity properties of the integrals.

3.2 Interface Problem

For the interface problems (2.5)-(2.8), the Green functions associated with the variable coefficients elliptic PDEs (2.5) and (2.6), respectively on subdomains Ω_i and Ω_e , are in general different.

Let $G_i(\mathbf{p}, \mathbf{q})$ be the Green function on the rectangle \mathcal{B} associated with the variable coefficients elliptic PDE (2.5) in Ω_i , which satisfies

$$\begin{aligned} \mathcal{A}_i G_i(\mathbf{p}, \mathbf{q}) &= \delta(\mathbf{p} - \mathbf{q}) && \text{in } \mathcal{B}, \\ G_i(\mathbf{p}, \mathbf{q}) &= 0 && \text{on } \partial\mathcal{B}. \end{aligned}$$

Let $G_e(\mathbf{p}, \mathbf{q})$ be the Green function on the rectangle \mathcal{B} associated with the variable coefficients elliptic PDE (2.6) in Ω_e , which satisfies

$$\begin{aligned} \mathcal{A}_e G_e(\mathbf{p}, \mathbf{q}) &= \delta(\mathbf{p} - \mathbf{q}) && \text{in } \mathcal{B}, \\ G_e(\mathbf{p}, \mathbf{q}) &= 0 && \text{on } \partial\mathcal{B}. \end{aligned}$$

Similar to those for the boundary value problems in the previous subsection, we also define the single layer, double layer, adjoint double layer and hyper-singular boundary integrals, associated with the differential operators \mathcal{A}_i and \mathcal{A}_e , respectively. Denote them by $\mathcal{L}_i, \mathcal{L}_e, \mathcal{M}_i, \mathcal{M}_e, \mathcal{M}_i^*, \mathcal{M}_e^*, \mathcal{N}_i$ and \mathcal{N}_e . For example,

$$\begin{aligned} \mathcal{L}_e \psi(\mathbf{p}) &\equiv \int_{\Gamma} G_e(\mathbf{q}, \mathbf{p}) \psi(\mathbf{q}) ds_{\mathbf{q}} \in H^{1/2}(\Gamma) && \text{for } \psi \in H^{-1/2}(\Gamma), \\ \mathcal{M}_e \varphi(\mathbf{p}) &\equiv \int_{\Gamma} \sigma_e(\mathbf{q}) \frac{\partial G_e(\mathbf{q}, \mathbf{p})}{\partial \mathbf{n}_{\mathbf{q}}} \varphi(\mathbf{q}) ds_{\mathbf{q}} \\ &= \int_{\Gamma} \sigma_e(\mathbf{q}) \mathbf{n}_{\mathbf{q}} \cdot \nabla_{\mathbf{q}} G(\mathbf{q}, \mathbf{p}) \varphi(\mathbf{q}) ds_{\mathbf{q}} \in H^{1/2}(\Gamma) && \text{for } \varphi \in H^{1/2}(\Gamma), \end{aligned} \tag{3.5}$$

and so on. Define the volume integral on Ω_e by

$$\mathcal{G}_e f_e(\mathbf{p}) \equiv \int_{\Omega_e} G_e(\mathbf{q}, \mathbf{p}) f_e(\mathbf{q}) d\mathbf{q}.$$

Let $\varphi = u_i$ and $\psi = \sigma_e \partial_{\mathbf{n}} u_e$ be two unknown density functions defined on Γ . By Green's (third) identities and the interface conditions (2.7), we have

$$\frac{1}{2} \varphi = \mathcal{M}_i \varphi - \mathcal{L}_i \psi - \mathcal{L}_i J + \mathcal{G}_i f_i \quad \text{on } \Gamma, \tag{3.6}$$

$$\frac{1}{2} (\varphi - g) = -\mathcal{M}_e \varphi + \mathcal{L}_e \psi + \mathcal{M}_e g + \mathcal{G}_e f_e \quad \text{on } \Gamma, \tag{3.7}$$

$$\frac{1}{2} (\psi + J) = \mathcal{N}_i \varphi - \mathcal{M}_i^* \psi - \mathcal{M}_i^* J + \sigma_i \partial_{\mathbf{n}} \mathcal{G}_i f_i \quad \text{on } \Gamma, \tag{3.8}$$

$$\frac{1}{2} \psi = -\mathcal{N}_e \varphi + \mathcal{M}_e^* \psi + \mathcal{N}_e g + \sigma_e \partial_{\mathbf{n}} \mathcal{G}_e f_e \quad \text{on } \Gamma. \tag{3.9}$$

Adding (3.6) to (3.7), (3.8) to (3.9), and making rearrangement of the terms, we reformulate the interface problem (2.5)-(2.8) as a system of two boundary integral equations, for $\mathbf{p} \in \Gamma$,

$$\varphi - (\mathcal{M}_i - \mathcal{M}_e) \varphi + (\mathcal{L}_i - \mathcal{L}_e) \psi = r(\mathbf{p}), \tag{3.10}$$

$$-(\mathcal{N}_i - \mathcal{N}_e) \varphi + \psi + (\mathcal{M}_i^* - \mathcal{M}_e^*) \psi = s(\mathbf{p}), \tag{3.11}$$

with

$$r(\mathbf{p}) = \frac{1}{2} g + \mathcal{G}_i f_i + \mathcal{G}_e f_e - \mathcal{L}_i J + \mathcal{M}_e g,$$

$$s(\mathbf{p}) = -\frac{1}{2} J + \sigma_i \partial_{\mathbf{n}_p} \mathcal{G}_i f_i + \sigma_e \partial_{\mathbf{n}_p} \mathcal{G}_e f_e - \mathcal{M}_i^* J + \mathcal{N}_e g.$$

After the densities, φ and ψ , are solved from the boundary integral equations, the potentials, u_i and u_e , are computed by evaluating the integrals below

$$u_i(\mathbf{p}) = \mathcal{M}_i \varphi - \mathcal{L}_i \psi - \mathcal{L}_i J + \mathcal{G}_i f_i \quad \text{in } \Omega_i, \tag{3.12}$$

$$u_e(\mathbf{p}) = -\mathcal{M}_e \varphi + \mathcal{L}_e \psi + \mathcal{M}_e g + \mathcal{G}_e f_e \quad \text{in } \Omega_e. \tag{3.13}$$

Finally, we remark that, in the case that $\kappa_e = \kappa_i = 0$ or $\sigma_e / \sigma_i = \kappa_e / \kappa_i$, for the interface problem (2.5)-(2.8), we may even get an equivalent boundary integral equation in the following form

$$\frac{1}{2} \psi(\mathbf{p}) + \mu \mathcal{M}_i^* \psi(\mathbf{p}) = \mu \mathcal{N}_i g + t(\mathbf{p}) \quad \text{on } \Gamma \tag{3.14}$$

with $\mu = (\sigma_e - \sigma_i) / (\sigma_e + \sigma_i) \in (-1, 1)$. Here, $t(\mathbf{p})$ is a linear combination of the known volume and boundary integrals.

4 The kernel-free boundary integral method

The kernel-free boundary integral method is a generalization of the standard boundary integral method and allows the solution of variable coefficients elliptic PDEs in the

formulation of boundary integral equations. As the Green function or the kernels of boundary integrals associated with variable coefficients elliptic PDEs are in general not analytically known, it is difficult if not impossible to directly evaluate the boundary integrals. The kernel-free boundary integral method replaces the evaluation of a boundary or volume integral by interpolation of a structured grid based solution, which satisfies a discrete equivalent interface problem on a larger regular box. The interface problem is solved with a fast solver. This section gives details of the method in two space dimensions ($d=2$).

4.1 Reinterpretation of the integrals

By the continuity properties of the boundary and volume integrals, we may reinterpret each of them as a solution to an equivalent interface problem.

For a piecewise smooth dependent variable $w(\mathbf{p})$, defined on the larger regular domain \mathcal{B} , which has possible discontinuities only on Γ , let $w^+(\mathbf{p})$ and $w^-(\mathbf{p})$ be the restrictions of $w(\mathbf{p})$ on the subdomains Ω_i and Ω_e , respectively. For $\mathbf{p} \in \Gamma$, we interpret $w^+(\mathbf{p})$ and $w^-(\mathbf{p})$ as the limit values of $w(\mathbf{p})$ from the corresponding side of the domain boundary. Assume the subdomain Ω_i is on the positive side of the boundary curve Γ while the subdomain Ω_e is on the negative side. The jump of the variable $v(\mathbf{p})$ across the boundary/interface Γ from negative to positive side is denoted by

$$[w(\mathbf{p})] \equiv w^+(\mathbf{p}) - w^-(\mathbf{p}) \quad \text{on } \Gamma.$$

In the following, we shall denote by $w_{i,e}$ the two cases for w_i and w_e , respectively.

The double layer potential $v(\mathbf{p}) = \mathcal{M}_{i,e}\varphi(\mathbf{p})$ satisfies the interface problem

$$\begin{aligned} \mathcal{A}_{i,e}v &\equiv \nabla \cdot (\sigma_{i,e}(\mathbf{p})\nabla v) - \kappa_{i,e}(\mathbf{p})v = 0 && \text{in } \mathcal{B} \setminus \Gamma, \\ [v] &= \varphi && \text{on } \Gamma, \\ \sigma_{i,e}[\partial_{\mathbf{n}}v] &= 0 && \text{on } \Gamma, \\ v &= 0 && \text{on } \partial\mathcal{B}. \end{aligned}$$

The single layer potential $v(\mathbf{p}) = -\mathcal{L}_{i,e}\psi(\mathbf{p})$ satisfies the interface problem

$$\begin{aligned} \mathcal{A}_{i,e}v &= \nabla \cdot (\sigma_{i,e}(\mathbf{p})\nabla v) - \kappa_{i,e}(\mathbf{p})v = 0 && \text{in } \mathcal{B} \setminus \Gamma, \\ [v] &= 0 && \text{on } \Gamma, \\ \sigma_{i,e}[\partial_{\mathbf{n}}v] &= \psi && \text{on } \Gamma, \\ v &= 0 && \text{on } \partial\mathcal{B}. \end{aligned}$$

The volume integral $v(\mathbf{p}) = \mathcal{G}_i f_i(\mathbf{p})$ satisfies the interface problem

$$\mathcal{A}_i v(\mathbf{p}) = \begin{cases} f_i & \text{if } \mathbf{p} \in \Omega_i, \\ 0 & \text{if } \mathbf{p} \in \Omega_e, \end{cases}$$

$$\begin{aligned} [v] &= 0 && \text{on } \Gamma, \\ \sigma_i [\partial_{\mathbf{n}} v] &= 0 && \text{on } \Gamma, \\ v &= 0 && \text{on } \partial\mathcal{B}. \end{aligned}$$

The volume integral $v(\mathbf{p}) = \mathcal{G}_e f_e(\mathbf{p})$ satisfies the interface problem

$$\begin{aligned} \mathcal{A}_e v(\mathbf{p}) &= \begin{cases} 0 & \text{if } \mathbf{p} \in \Omega_i, \\ f_e & \text{if } \mathbf{p} \in \Omega_e, \end{cases} \\ [v] &= 0 && \text{on } \Gamma, \\ \sigma_e [\partial_{\mathbf{n}} v] &= 0 && \text{on } \Gamma, \\ v &= 0 && \text{on } \partial\mathcal{B}. \end{aligned}$$

Remark 4.1. The equivalences between the interface problems and the volume, boundary integrals are illustrated and proved in the appendix.

4.2 Discretization of the PDE on a Cartesian grid

In this and the next sections, we will omit the subscripts for the interior and exterior variables. We discretize the PDE

$$\mathcal{A}v \equiv \nabla \cdot (\sigma(\mathbf{p}) \nabla v) - \kappa(\mathbf{p})v = f(\mathbf{p}) \quad \text{in } \mathcal{B} \setminus \Gamma \tag{4.1}$$

on a Cartesian grid with finite difference method. Here, the differential operator \mathcal{A} uses only one set of coefficients, $\{\sigma_i, \kappa_i\}$ or $\{\sigma_e, \kappa_e\}$, throughout the rectangle \mathcal{B} ; the source term $f(\mathbf{p})$ may vanish on one side of the interface Γ , depending on the operator among \mathcal{A}_i and \mathcal{A}_e which \mathcal{A} stands for.

In two space dimensions, for simplicity, assume the box $\mathcal{B} = (a, b) \times (c, d)$ is a square. Let $M > 1$ be an integer and $h = (b - a) / M = (d - c) / M$ be a mesh parameter. For $i, j = 0, 1, \dots, M$, let $x_i = a + ih$ and $y_j = c + jh$. The box \mathcal{B} is partitioned into a uniform grid with nodes $\{\mathbf{p}_{i,j} = (x_i, y_j)\}_{i,j=0}^M$. With the second-order centered finite difference method, the elliptic PDE (4.1) is discretized into the finite difference equations

$$\mathcal{A}_h v_{i,j} \equiv \frac{s_{i,j} - 4\bar{\sigma}_{i,j} v_{i,j}}{h^2} - \kappa_{i,j} v_{i,j} = f_{i,j}, \tag{4.2}$$

with

$$s_{i,j} = \sigma_{i+1/2,j} v_{i+1,j} + \sigma_{i-1/2,j} v_{i-1,j} + \sigma_{i,j+1/2} v_{i,j+1} + \sigma_{i,j-1/2} v_{i,j-1},$$

for $i, j = 1, 2, \dots, M - 1$. Here, $v_{i,j}$ is the finite difference approximation of $v(\mathbf{p}_{i,j})$; $\sigma_{i+1/2,j} = \sigma(x_i + h/2, y_j)$, $\sigma_{i,j+1/2} = \sigma(x_i, y_j + h/2)$, $\kappa_{i,j} = \kappa(x_i, y_j)$, $f_{i,j} = f(x_i, y_j)$ and $\bar{\sigma}_{i,j} = (\sigma_{i+1/2,j} + \sigma_{i-1/2,j} + \sigma_{i,j+1/2} + \sigma_{i,j-1/2}) / 4$. At each grid node $\mathbf{p}_{i,j} = (x_i, y_j)$, the finite difference equation involves a five-point stencil. In the absence of interface Γ , provided that the coefficients $\sigma(\mathbf{p})$, $\kappa(\mathbf{p})$ and the data $f(\mathbf{p})$ are sufficiently smooth, the solution to the finite difference equation (4.2) has second-order accuracy.

4.3 Correction of the discrete system

The grid nodes $\{\mathbf{p}_{i,j} = (x_i, y_j)\}_{i,j=0}^M$ are classified into regular and irregular nodes. Those at which the five-point stencil of the finite difference equation (4.2) has intersection with the boundary/interface Γ are called irregular grid nodes; others are called regular grid nodes.

Due to the discontinuities of the solution and/or its normal derivative across the interface Γ , the finite difference approximation (4.2) at irregular grid nodes has much larger local truncation errors than those at regular grid nodes. Precisely, we have the following estimate for the local truncation errors,

$$\mathcal{A}_h v(x_i, y_j) - f(x_i, y_j) = \begin{cases} \mathcal{O}(h^2) & \text{if } (x_i, y_j) \text{ is a regular node,} \\ \mathcal{O}(h^{-2}) & \text{if } (x_i, y_j) \text{ is an irregular node.} \end{cases}$$

Here, $v(\mathbf{p}) = v(x, y)$ is the solution to the elliptic PDE (4.1), subject to two interface conditions on Γ ; $\mathcal{A}_h v(x_i, y_j)$ is obtained by replacing the approximate values $v_{i,j}$ with the values of $v(x, y)$ at grid nodes $\mathbf{p}_{i,j} = (x_i, y_j)$.

As the local truncation errors at irregular grid nodes are too large, the solution to the finite difference equation (4.2) will be inaccurate. The finite difference equation (4.2) must be corrected for the solution to the modified system to have formal second-order accuracy.

For simplicity, we first consider the case when the five-point finite difference stencil at irregular grid node (x_i, y_j) intersects the boundary/interface on the horizontal grid line only once while keeping in mind that the finite difference stencil may intersect the horizontal line twice. Assume the line segment connecting nodes (x_i, y_j) and (x_{i+1}, y_j) intersects the interface at point (z_i, y_j) (see Fig. 2) with $x_i \leq z_i < x_{i+1}$. Denote the smooth solution on the left and right hand sides of the interface by $v^-(\mathbf{p})$ and $v^+(\mathbf{p})$, respectively.

In the next, we will estimate the horizontal part of the local truncation error

$$E_{h,x}(x_i, y_j) \equiv \frac{\sigma_{i+1/2,j}(v^+(x_{i+1}, y_j) - v^-(x_i, y_j))}{h^2} - \frac{\sigma_{i-1/2,j}(v^-(x_i, y_j) - v^-(x_{i-1}, y_j))}{h^2} - \frac{\partial}{\partial x} \left(\sigma \frac{\partial}{\partial x} v^-(x_i, y_j) \right). \quad (4.3)$$

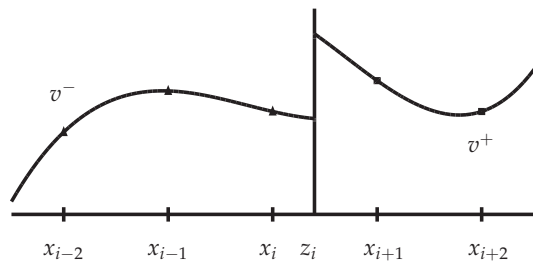


Figure 2: Piecewise smooth function along a line with an interface.

First we make Taylor expansions for $v^\pm(x, y_j)$ around the point (z_i, y_j) ,

$$v^\pm(x_{i+1}, y_j) = v^\pm(z_i, y_j) + \partial_x v^\pm(z_i, y_j)(x_{i+1} - z_i) + \frac{1}{2} \partial_{xx} v^\pm(z_i, y_j)(x_{i+1} - z_i)^2 + \frac{1}{6} \partial_{xxx} v^\pm(z_i, y_j)(x_{i+1} - z_i)^3 + \mathcal{O}(h^4).$$

Note that, with the expansions, we may estimate the leading order term of $E_{h,x}(x_i, y_j)$ by

$$E_{h,x}^+(x_i, y_j) \equiv \frac{\sigma_{i+1/2,j}}{h^2} (v^+(x_{i+1}, y_j) - v^-(x_{i+1}, y_j)) = \frac{\sigma_{i+1/2,j}}{h^2} \left\{ [v] + [v_x](x_{i+1} - z_i) + \frac{1}{2} [v_{xx}](x_{i+1} - z_i)^2 + \frac{1}{6} [v_{xxx}](x_{i+1} - z_i)^3 \right\} + \mathcal{O}(h^2).$$

Here, $[v] = v^+(z_i, y_j) - v^-(z_i, y_j)$, $[\partial_x v] = \partial_x v^+(z_i, y_j) - \partial_x v^-(z_i, y_j)$, $[v_{xx}] = \partial_{xx} v^+(z_i, y_j) - \partial_{xx} v^-(z_i, y_j)$ and $[v_{xxx}] = \partial_{xxx} v^+(z_i, y_j) - \partial_{xxx} v^-(z_i, y_j)$ are the jumps of the function and its partial derivatives across the interface.

Thus, we see the horizontal part $E_{h,x}(x_i, y_j)$ of the local truncation error can be approximated by the following quantity

$$C_{h,x}^+(x_i, y_j) \equiv \frac{\sigma_{i+1/2,j}}{h^2} \left\{ [v] + [v_x](x_{i+1} - z_i) + \frac{1}{2} [v_{xx}](x_{i+1} - z_i)^2 \right\},$$

which introduces a first-order error, since

$$E_{h,x}(x_i, y_j) = E_{h,x}^+(x_i, y_j) + \mathcal{O}(h^2) = C_h^+(x_i, y_j) + \mathcal{O}(h).$$

The correction $C_{h,x}^+(x_i, y_j)$ is computable once the jumps $[v]$, $[v_x]$ and $[v_{xx}]$ are known. As a matter of fact, the jumps of the partial derivatives of function v can be calculated from the jumps of the function and its normal derivative. Details of the calculation are presented in Subsection 4.6.

In the case that the boundary/interface Γ intersects the line segment connecting nodes (x_{i-1}, y_j) and (x_i, y_j) at point (z_i, y_j) with $x_{i-1} \leq z_i < x_i$, the modification for the finite difference equation at irregular grid node (x_i, y_j) should take into account the computable quantity below

$$C_{h,x}^-(x_i, y_j) \equiv -\frac{\sigma_{i-1/2,j}}{h^2} \left\{ [v] + [v_x](x_{i-1} - z_i) + \frac{1}{2} [v_{xx}](x_{i-1} - z_i)^2 \right\}.$$

In the case that the five-point finite difference stencil at point (x_i, y_j) intersects the boundary/interface Γ at the vertical line segments, similar computable quantities $C_{h,y}^+(x_i, y_j)$ and $C_{h,y}^-(x_i, y_j)$ can be derived.

In general, at an irregular grid node (x_i, y_j) , the interface may intersect the five-point finite difference stencil multiple times. We need to add the corresponding terms among

$C_{h,x}^+$, $C_{h,x}^-$, $C_{h,y}^+$ and $C_{h,y}^-$ for modifying the right hand side of the finite difference equation. Denote by $C_h(x_i, y_j)$ the sum of all correction contributions from different intersected points. Now we modify the finite difference equation (4.2) to be

$$\mathcal{A}_h v_{i,j} = \begin{cases} f_{i,j} & \text{if } (x_i, y_j) \text{ is a regular point,} \\ f_{i,j} + C_h(x_i, y_j) & \text{if } (x_i, y_j) \text{ is an irregular point,} \end{cases} \quad (4.4)$$

for $i, j = 1, 2, \dots, M-1$.

With the correction, the local truncation error of the finite difference equation at irregular grid nodes is of first order

$$\mathcal{A}_h v_h(x_i, y_j) - f(x_i, y_j) - C_h(x_i, y_j) = \mathcal{O}(h)$$

if (x_i, y_j) is an irregular point. It is known [5, 48] that the solution to the corrected linear system (4.4) has essentially second-order accuracy.

4.4 Solution of the discrete interface equations

In the previous subsection, we see that the finite difference equation for the interface problem on a Cartesian grid is modified for the solution to the resulting linear system to have essential second-order accuracy [5, 48]. A good point of the modification is that the correction is only made to the right hand side of the linear system while the coefficient matrix remains the same as the smooth case, the symmetry and positive or negative definiteness being preserved.

For constant coefficients linear elliptic operators such as the Laplacian or the modified Helmholtz operator, the modified finite difference equation (4.4) can be solved by a fast Fourier transform based elliptic PDE solver.

In this work, for the variable coefficients elliptic operators, the modified finite difference equation (4.4) is solved by a geometric multigrid type method, assuming the Cartesian grid results from a sequence of uniform refinement (bisection) for the box \mathcal{B} .

Denote by \mathcal{T}_h the Cartesian grid with mesh parameter h for the box \mathcal{B} . Assume it is generated from uniform bisection of the coarse grid \mathcal{T}_{2h} with double-size mesh parameter.

The modified finite difference equation (4.4) on grid \mathcal{T}_h is solved with a geometric multigrid preconditioned conjugate gradient (GMG-PCG) iteration. The multigrid preconditioner is a standard V-cycle, consisting of pre-smoothing, residual restriction, coarser grid iteration, correction prolongation and post-smoothing. The pre-smoothing and post-smoothing is made by one forward and one backward Gauss-Seidel iteration, respectively. The prolongation is computed by bi-linear interpolation while the restriction is simply implemented as the adjoint of the prolongation. The coarsest grid for the box \mathcal{B} has only two by two grid cells and one interior grid node, which implies that the system on the coarsest grid has only a single finite difference equation.

If a coarser grid \mathcal{T}_{2h} exists, the initial guess for the GMG-PCG iteration is obtained by linear interpolation of the numerical solution to the finite difference equation on the

coarser grid \mathcal{T}_{2h} , which is also solved with the GMG-PCG iterative method. This process is recursive. The resulting iterative method for the modified finite difference equation is in fact a full GMG-PCG iterative method.

4.5 Interpolation for integral values on the boundary

Let $v_h(\mathbf{p})$ be a sufficiently smooth function defined in $\mathcal{B} \setminus \Gamma$ so that the action of the elliptic differential operator \mathcal{A} on it is meaningful. The function and its partial derivatives are possibly discontinuous only on the boundary/interface Γ . Assume the piecewise smooth function $v_h(\mathbf{p})$ satisfies the interface conditions and $v_h(\mathbf{p}_{i,j}) = v_{i,j}$, where $v_{i,j}$ is the numerical solution to the finite difference equation (4.2). By the assumption, we may also call $v_h(\mathbf{p})$ as an approximate solution to the corresponding interface problem.

Let v_h^+ and v_h^- be restrictions of v_h on the subdomains Ω_i and Ω_e , respectively. Taylor expansion of the approximate solution $v_h(\mathbf{p})$ around a point \mathbf{q} on Γ (see Fig. 3) gives us

$$\begin{aligned}
 v_h(\mathbf{p}) = & v_h^+(\mathbf{q}) + \frac{\partial v_h^+(\mathbf{q})}{\partial x} \xi + \frac{\partial v_h^+(\mathbf{q})}{\partial y} \eta + \frac{1}{2} \frac{\partial^2 v_h^+(\mathbf{q})}{\partial x^2} \xi^2 \\
 & + \frac{\partial^2 v_h^+(\mathbf{q})}{\partial x \partial y} \xi \eta + \frac{1}{2} \frac{\partial^2 v_h^+(\mathbf{q})}{\partial y^2} \eta^2 + \mathcal{O}(|\mathbf{p} - \mathbf{q}|^3) \quad \text{if } \mathbf{p} \in \Omega_i, \quad (4.5)
 \end{aligned}$$

and

$$\begin{aligned}
 v_h(\mathbf{p}) = & v_h^-(\mathbf{q}) + \frac{\partial v_h^-(\mathbf{q})}{\partial x} \xi + \frac{\partial v_h^-(\mathbf{q})}{\partial y} \eta + \frac{1}{2} \frac{\partial^2 v_h^-(\mathbf{q})}{\partial x^2} \xi^2 \\
 & + \frac{\partial^2 v_h^-(\mathbf{q})}{\partial x \partial y} \xi \eta + \frac{1}{2} \frac{\partial^2 v_h^-(\mathbf{q})}{\partial y^2} \eta^2 + \mathcal{O}(|\mathbf{p} - \mathbf{q}|^3) \quad \text{if } \mathbf{p} \in \Omega_e. \quad (4.6)
 \end{aligned}$$

Here, $(\xi, \eta)^T \equiv \mathbf{p} - \mathbf{q}$. For conciseness, we denote the limit values of the approximate

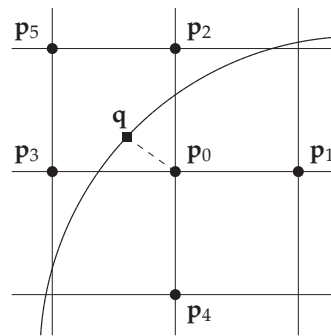


Figure 3: Six grid nodes \mathbf{p}_j ($j=0,1,\dots,5$) for computing the limit values of an approximate solution and its derivatives at point \mathbf{q} .

solution $v_h(\mathbf{p})$ and its derivatives by

$$V^\pm \equiv v_h^\pm(\mathbf{q}), \quad V_x^\pm \equiv \frac{\partial v_h^\pm(\mathbf{q})}{\partial x}, \quad V_y^\pm \equiv \frac{\partial v_h^\pm(\mathbf{q})}{\partial y},$$

and

$$V_{xx}^\pm \equiv \frac{\partial^2 v_h^\pm(\mathbf{q})}{\partial x^2}, \quad V_{xy}^\pm \equiv \frac{\partial^2 v_h^\pm(\mathbf{q})}{\partial x \partial y}, \quad V_{yy}^\pm \equiv \frac{\partial^2 v_h^\pm(\mathbf{q})}{\partial y^2}.$$

Evaluating the truncated Taylor series, (4.5) or (4.6), at six nearby grid nodes \mathbf{p}_j ($j = 0, 1, \dots, 5$) (see Fig. 3) yields

$$V^+ + V_x^+ \zeta_j + V_y^+ \eta_j + \frac{1}{2} \zeta_j^2 V_{xx}^+ + \zeta_j \eta_j V_{xy}^+ + \frac{1}{2} \eta_j^2 V_{yy}^+ = V_j \quad \text{if } \mathbf{p}_j \in \Omega_i \tag{4.7}$$

and

$$V^- + V_x^- \zeta_j + V_y^- \eta_j + \frac{1}{2} \zeta_j^2 V_{xx}^- + \zeta_j \eta_j V_{xy}^- + \frac{1}{2} \eta_j^2 V_{yy}^- = V_j \quad \text{if } \mathbf{p}_j \in \Omega_e, \tag{4.8}$$

with $V_j \equiv v_h(\mathbf{p}_j)$ and $(\zeta_j, \eta_j)^T \equiv \mathbf{p}_j - \mathbf{q}$, for $j = 0, 1, \dots, 5$. Let

$$J_j \equiv [V] + \zeta_j [V_x] + \eta_j [V_y] + \frac{1}{2} \zeta_j^2 [V_{xx}] + \zeta_j \eta_j [V_{xy}] + \frac{1}{2} \eta_j^2 [V_{yy}].$$

Using the jump relations of the solution and its derivatives, we rewrite (4.8) as

$$V^+ + V_x^+ \zeta_j + V_y^+ \eta_j + \frac{1}{2} \zeta_j^2 V_{xx}^+ + \zeta_j \eta_j V_{xy}^+ + \frac{1}{2} \eta_j^2 V_{yy}^+ = V_j + J_j \quad \text{if } \mathbf{p}_j \in \Omega_e. \tag{4.9}$$

Let $a_j \equiv \zeta_j/h$, $b_j \equiv \eta_j/h$ and introduce new quantities:

$$W^\pm \equiv V^\pm, \quad W_a^\pm \equiv h V_x^\pm, \quad W_b^\pm \equiv h V_y^\pm,$$

and

$$W_{aa}^\pm \equiv h^2 V_{xx}^\pm, \quad W_{ab}^\pm \equiv h^2 V_{xy}^\pm, \quad W_{bb}^\pm \equiv h^2 V_{yy}^\pm.$$

Then from Eqs. (4.7) and (4.9), we obtain

$$W^+ + a_j W_a^+ + b_j W_b^+ + \frac{1}{2} a_j^2 W_{aa}^+ + a_j b_j W_{ab}^+ + \frac{1}{2} b_j^2 W_{bb}^+ = V_j \quad \text{if } \mathbf{p}_j \in \Omega_i \tag{4.10}$$

or

$$W^+ + a_j W_a^+ + b_j W_b^+ + \frac{1}{2} a_j^2 W_{aa}^+ + a_j b_j W_{ab}^+ + \frac{1}{2} b_j^2 W_{bb}^+ = V_j + J_j \quad \text{if } \mathbf{p}_j \in \Omega_e \tag{4.11}$$

for $j=0, 1, \dots, 5$. Note that the coefficient matrix of the linear system consisting of Eqs. (4.10)-(4.11) is independent of the mesh parameter h . The limit values of the approximate solution and its derivatives are uniquely determined by (4.10)-(4.11) if we appropriately choose the six grid nodes \mathbf{p}_j ($j = 0, 1, \dots, 5$) such that the coefficient matrix is invertible.

For a point $\mathbf{q} \in \Gamma$, the six points $\{\mathbf{p}_j\}_{j=0}^5$ for the interpolation are chosen as follows. First, the closest node \mathbf{p}_0 on the Cartesian grid \mathcal{T}_h is selected. Then the four neighboring grid nodes $\{\mathbf{p}_i\}_{i=1}^4$ as shown in Fig. 3 are added into the interpolation stencil. Finally, the sixth grid node \mathbf{p}_5 is chosen to be the closest grid node on a diagonal line passing through node \mathbf{p}_0 that is on the same quadrant as point \mathbf{q} (see Fig. 3).

4.6 Calculation for jumps of partial derivatives

Assume function $v(\mathbf{p})$ is smooth in \mathcal{B} except on the interface Γ and satisfies the interface problem

$$\mathcal{A}v \equiv \nabla \cdot (\sigma \nabla v) - \kappa v = f \quad \text{in } \mathcal{B}, \tag{4.12}$$

$$[v] = \varphi \quad \text{on } \Gamma, \tag{4.13}$$

$$\sigma [\partial_{\mathbf{n}} v] = \psi \quad \text{on } \Gamma. \tag{4.14}$$

This section describes the calculation for the jumps of partial derivatives of $v(\mathbf{p})$ in terms of the jumps of the function and its normal derivative, $[v]$ and $\sigma [\partial_{\mathbf{n}} v]$.

Let $\boldsymbol{\tau}$ be a tangent vector at a point on the interface. Taking tangential derivative of the interface condition (4.13) along $\boldsymbol{\tau}$ yields

$$\partial_{\boldsymbol{\tau}} [v] = \partial_{\boldsymbol{\tau}} \varphi \quad \text{on } \Gamma. \tag{4.15}$$

The two equations (4.14)-(4.15) will uniquely determine the jumps of the first-order partial derivatives: $[v_x]$ and $[v_y]$.

Taking tangential derivative of interface condition (4.14) along the tangential direction $\boldsymbol{\tau}$ yields

$$\partial_{\boldsymbol{\tau}} \{ \sigma [\partial_{\mathbf{n}} v] \} = \partial_{\boldsymbol{\tau}} \psi \quad \text{on } \Gamma. \tag{4.16}$$

Taking tangential derivative of condition (4.15) yields

$$\partial_{\boldsymbol{\tau}\boldsymbol{\tau}} [v] = \partial_{\boldsymbol{\tau}\boldsymbol{\tau}} \varphi \quad \text{on } \Gamma. \tag{4.17}$$

The elliptic PDE (4.12) implies

$$[\nabla \cdot (\sigma \nabla v)] - \kappa [v] = [f] \quad \text{on } \Gamma. \tag{4.18}$$

The three equations (4.16)-(4.18) will determine the jumps of the second-order partial derivatives: $[v_{xx}]$, $[v_{yy}]$, $[v_{xy}]$.

Let s be an independent variable for the local parametric representation of boundary Γ , assuming

$$x = x(s) \quad \text{and} \quad y = y(s).$$

Let

$$\mathbf{r} = (x, y)^T, \quad \boldsymbol{\tau} = \frac{\partial \mathbf{r}}{\partial s}$$

and n_1, n_2 be the components of the unit outward normal vector \mathbf{n} at a point on Γ .

Eqs. (4.14)-(4.15) explicitly read

$$\begin{aligned} n_1 [v_x] + n_2 [v_y] &= \psi / \sigma, \\ \frac{\partial x}{\partial s} [v_x] + \frac{\partial y}{\partial s} [v_y] &= \varphi_s. \end{aligned}$$

Solving the two by two linear system yields the jumps of the first partial derivatives, $[v_x]$ and $[v_y]$.

Eqs. (4.16)-(4.18) explicitly read

$$\begin{aligned} n_1 \frac{\partial x}{\partial s} [v_{xx}] + n_2 \frac{\partial y}{\partial s} [v_{yy}] + \left(n_1 \frac{\partial y}{\partial s} + n_2 \frac{\partial x}{\partial s} \right) [v_{xy}] &= r_1, \\ \left(\frac{\partial x}{\partial s} \right)^2 [v_{xx}] + \left(\frac{\partial y}{\partial s} \right)^2 [v_{yy}] + 2 \frac{\partial x}{\partial s} \frac{\partial y}{\partial s} [v_{xy}] &= r_2, \\ [v_{xx}] + [v_{yy}] &= r_3, \end{aligned}$$

with

$$\begin{aligned} r_1 &= \frac{\psi_s}{\sigma} - \frac{\sigma_s}{\sigma} \{ n_1 [v_x] + n_2 [v_y] \} - \frac{\partial n_1}{\partial s} [v_x] - \frac{\partial n_2}{\partial s} [v_y], \\ r_2 &= \varphi_{ss} - \frac{\partial^2 x}{\partial s^2} [v_x] - \frac{\partial^2 y}{\partial s^2} [v_y], \\ r_3 &= \{ \kappa [v] - \sigma_x [v_x] - \sigma_y [v_y] + [f] \} / \sigma. \end{aligned}$$

Solving the linear system consisting of the three equations above yields the jumps of the second-order partial derivatives, $[v_{xx}]$, $[v_{yy}]$ and $[v_{xy}]$.

5 Algorithm summary

Suppose that the boundary integral equation (3.1), (3.3) or (3.10)-(3.11), respectively corresponding to the boundary value problems (2.1)-(2.2), (2.3)-(2.4) or the general interface problem (2.5)-(2.8), is solved with a Krylov subspace method after space discretization. During the iteration, evaluation of the volume integral and boundary integral(s) with the iterated density or densities are made by solving the corresponding equivalent simple interface problems in Subsection 4.1. Each integral that appears in the BIEs (3.10)-(3.11) is computed separately in the whole box \mathcal{B} with one corresponding set of coefficients, either interior or exterior. The simple interface problems in Subsection 4.1 are solved using Subsections 4.2-4.4. The correction in Subsection 4.3 for the discrete interface equations needs the jumps of partial derivatives, which are computed by the method presented in Subsection 4.6. After the discrete equations are solved, the grid based solution is interpolated to the interface using Subsection 4.5, which also needs the jumps of partial derivatives calculated by the method in Subsection 4.6. After the boundary integral equation is solved, the solution to the boundary value problem or the general interface problem (2.5)-(2.8) can be correspondingly obtained by (3.2), (3.4) or (3.12)-(3.13).

6 Numerical examples

This section presents examples for the boundary value and interface problems of variable coefficients elliptic PDEs in two space dimensions ($d=2$) with the kernel-free boundary integral method.

For the boundary integral method, the boundary or interface may be explicitly represented with a parametric or spline curve [48] or implicitly represented by the intersection points of a Cartesian grid with the zero level set of a smooth function [49]. The examples below adapt the latter approach. The boundary representation method involves a parameter α , called overlapping surface decomposition parameter. It is fixed to be $\alpha = \pi/3$ in this work (refer to [49] for details).

The discrete boundary integral equations in all the numerical experiments (Examples 6.1-6.7) are solved with the generalized minimal residual (GMRES) iterative method [42]. For the iteration, the unknown densities are initialized with twice the boundary data for the boundary value problems and zeros for the interface problems. The GMRES iteration stops when the iterated residual in the discrete ℓ^2 -norm relative to that of the initial residual is less than a prescribed tolerance $\epsilon_{bie} = 10^{-8}$.

In Examples 6.1-6.2 and 6.6-6.7, the modified finite difference equations are solved with the full multigrid-preconditioned conjugate gradient method. In Examples 6.3-6.5, where the PDEs have constant coefficients, the modified finite difference equations are computed with the fast Fourier transform based fast Poisson solver.

The full multigrid-preconditioned conjugate gradient method for the modified finite difference equation in Examples 6.1-6.2 and 6.6-6.7 stops when the iterated residual in the discrete ℓ^2 -norm relative to that of the initial one is less than the tolerance $\epsilon_{fdm} = 10^{-10}$.

Numerical results for the examples are listed in Tables 1-19. In each table, the first column has the grid sizes; the second column has the number of GMRES iterations. In Tables 1 and 2 for the Dirichlet and Neumann BVPs, the third and fourth columns have the errors of the numerical solutions in the discrete ℓ^2 -norm and the discrete maximum norm. In other tables for the interface problems, the third and fourth columns have the errors of the numerical solutions inside and outside the interface in the discrete maximum norm. In each of Tables 1-19, the last column lists the CPU times in seconds used by the computer for the corresponding numerical experiments.

The kernel-free boundary integral method proposed in this work was implemented in custom codes written in the C++ computer language. The numerical experiments were all performed in double precision on a computer with Intel(R) Xeon(R) 2.93GHz CPU.

Example 6.1. This one solves the Dirichlet BVP (2.1)-(2.2) with spatially variable coefficients

$$\sigma_i(x,y) = 2 + \sin \pi(x+y) \quad \text{and} \quad \kappa_i(x,y) = x^2 + y^2.$$

The Dirichlet boundary data $g(x,y)$ and source data $f(x,y)$ are chosen such that the exact solution to the problem is given by $u(x,y) = \exp(\pi x) \cos(\pi y)$. The computational domain Ω_i is an ellipse with major and minor radius respectively equal to 0.8 and 0.4, rotated counterclockwise by 30 degrees (See Fig. 4). The larger rectangle \mathcal{B} is given by $(-1,1) \times (-1,1)$. Fig. 4 shows the isolines of a numerical solution to the boundary integral equation (3.1) for the Dirichlet BVP. The numerical results in Table 1 verify that the GMRES iteration number is essentially independent of the mesh parameter and the KFBI method yields second-order accurate solutions.

Table 1: Numerical results for the Dirichlet BVP of Example 6.1.

grid size	#GMRES	$\ e_h\ _{\ell^2}$	$\ e_h\ _{\infty}$	CPU times
128×128	8	1.95E-4	4.19E-4	0.15
256×256	8	4.85E-5	1.02E-4	0.68
512×512	8	1.24E-5	2.58E-5	4.64
1024×1024	8	3.07E-6	6.43E-6	23.3
2048×2048	8	7.39E-7	1.58E-6	106.1

Example 6.2. This one solves the Neumann BVP (2.3)-(2.4) with spatially variable coefficients

$$\sigma_i(x,y) = 2 + \sin \pi(x+y) \quad \text{and} \quad \kappa_i(x,y) = 0.$$

The Neumann boundary data $g^N(x,y)$ and source data $f(x,y)$ are chosen such that the exact solution to the problem is given by $u(x,y) = \exp(\pi x) \cos(\pi y)$, too. The computational domain Ω_i and the larger regular box \mathcal{B} are also the same as Example 6.1. The solution to the pure Neumann BVP is not unique. To fix a unique solution, we translate the numerical solution so that it matches with the exact one at the origin. Fig. 5 shows the isolines of a numerical solution to the boundary integral equation (3.3) for the Neumann BVP. The numerical results in Table 2 verify that the GMRES iteration number is also essentially independent of the mesh parameter and the KFBI method for the Neumann BVP yields second-order accurate solutions, too.

Table 2: Numerical results for the Neumann BVP of Example 6.2.

grid size	#GMRES	$\ e_h\ _{\ell^2}$	$\ e_h\ _{\infty}$	CPU times
128×128	9	1.26E-3	5.77E-3	0.13
256×256	9	3.06E-4	1.53E-3	0.58
512×512	8	4.32E-5	2.25E-4	3.43
1024×1024	8	1.69E-5	8.56E-5	17.2
2048×2048	8	2.57E-6	1.31E-5	70.7

Example 6.3. In this example, we consider the interface problem with piecewise constant coefficients below

$$\begin{aligned} \sigma_i \Delta u_i &= f_i & \text{in } \Omega_i, \\ \sigma_e \Delta u_e &= f_e & \text{in } \Omega_e, \end{aligned}$$

subject to two interface conditions

$$u_i - u_e = g \quad \text{and} \quad \sigma_i \partial_{\mathbf{n}} u_i - \sigma_e \partial_{\mathbf{n}} u_e = j \quad \text{on } \Gamma$$

and the boundary condition

$$u_e = 0 \quad \text{on } \partial \mathcal{B}$$

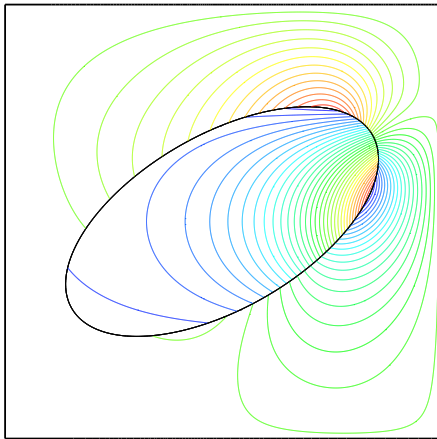


Figure 4: Isolines of a numerical solution to the Dirichlet BVP of Example 6.1.

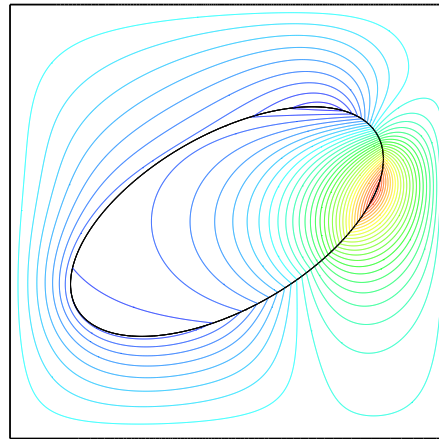


Figure 5: Isolines of a numerical solution to the Neumann BVP of Example 6.2.

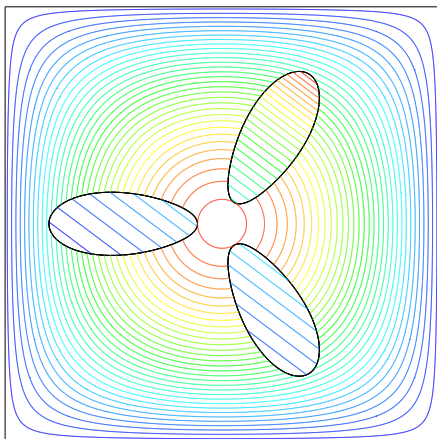


Figure 6: Isolines of a numerical solution to the interface problem of Example 6.3.

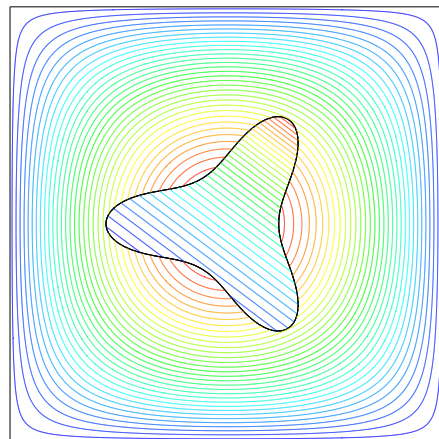


Figure 7: Isolines of a numerical solution to the interface problem of Example 6.4.

with the kernel-free boundary integral method. The interface Γ is given by the zero level set of the smooth function

$$\Theta(x,y) = (x^2 + y^2) \left(x^2 + y^2 + \frac{4}{5}x \right) - \frac{16}{5}xy^2 + \frac{1}{1000}.$$

That is, $\Gamma = \{(x,y) \in \mathbb{R}^2 : \Theta(x,y) = 0\}$. It has three disconnected components, as illustrated in Fig. 6. The larger rectangle, which embeds the interface Γ , is also the square centered at the origin with radius equal to one, $\mathcal{B} = (-1,1)^2$. The interface conditions, g and j , and the source terms f_i and f_e for the interface problem are chosen so that the exact solution reads

Table 3: Numerical results for the interface problem of Example 6.3 ($\sigma_i=1$ and $\sigma_e=25$).

grid size	#GMRES	$\ e_h\ _{\infty,\Omega_i}$	$\ e_h\ _{\infty,\Omega_e}$	CPU times
256×256	11	1.25E-4	3.34E-5	0.48
512×512	11	1.01E-5	2.63E-6	1.79
1024×1024	11	2.47E-6	1.00E-6	7.87
2048×2048	11	3.33E-7	1.51E-7	35.7

Table 4: Numerical results for the interface problem of Example 6.3 ($\sigma_i=1$ and $\sigma_e=50$).

grid size	#GMRES	$\ e_h\ _{\infty,\Omega_i}$	$\ e_h\ _{\infty,\Omega_e}$	CPU times
256×256	11	1.31E-4	3.45E-5	0.39
512×512	11	1.01E-5	2.62E-6	1.51
1024×1024	11	2.47E-6	9.86E-7	6.60
2048×2048	11	3.07E-7	1.56E-7	31.8

Table 5: Numerical results for the interface problem of Example 6.3 ($\sigma_i=1$ and $\sigma_e=100$).

grid size	#GMRES	$\ e_h\ _{\infty,\Omega_i}$	$\ e_h\ _{\infty,\Omega_e}$	CPU times
256×256	11	1.42E-4	3.52E-5	0.38
512×512	11	1.02E-5	2.61E-6	1.50
1024×1024	11	2.52E-6	9.77E-7	6.61
2048×2048	11	2.83E-7	1.59E-7	31.9

Table 6: Numerical results for the interface problem of Example 6.3 ($\sigma_i=1$ and $\sigma_e=200$).

grid size	#GMRES	$\ e_h\ _{\infty,\Omega_i}$	$\ e_h\ _{\infty,\Omega_e}$	CPU times
256×256	12	1.73E-4	3.54E-5	0.41
512×512	12	9.95E-6	2.60E-6	1.59
1024×1024	12	2.39E-6	9.67E-7	7.08
2048×2048	12	3.40E-7	1.48E-7	34.0

$$\begin{aligned}
 u_i(x,y) &= \exp(0.6x+0.8y) && \text{for } (x,y) \in \Omega_i, \\
 u_e(x,y) &= \sin(\pi(x+1)/2) \sin(\pi(y+1)/2) && \text{for } (x,y) \in \Omega_e.
 \end{aligned}$$

Fig. 6 shows the isolines of a numerical solution to the boundary integral equations (3.10)-(3.11) for the interface problem with the KFBI method. Tables 3-8 contain numerical results from solving the BIEs (3.10)-(3.11) for the interface problem with the piecewise constant coefficients, different tables corresponding to different coefficient ratios. The ratio of coefficients ranges from 1:25 to 1:20000. The GMRES iteration numbers in the tables show that the efficiency of the KFBI method for the interface problem is insensitive to the ratio of coefficients, in fact due to the well-conditioning of the boundary integral equation (3.14). When the ratio of the diffusion coefficients is moderately large, the numerical

Table 7: Numerical results for the interface problem of Example 6.3 ($\sigma_i=1$ and $\sigma_e=2000$).

grid size	#GMRES	$\ e_h\ _{\infty,\Omega_i}$	$\ e_h\ _{\infty,\Omega_e}$	CPU times
256×256	12	8.63E-4	3.57E-5	0.42
512×512	12	1.01E-5	2.60E-6	1.62
1024×1024	12	2.22E-6	9.62E-7	7.15
2048×2048	12	3.32E-7	1.49E-7	34.0

Table 8: Numerical results for the interface problem of Example 6.3 ($\sigma_i=1$ and $\sigma_e=20000$).

grid size	#GMRES	$\ e_h\ _{\infty,\Omega_i}$	$\ e_h\ _{\infty,\Omega_e}$	CPU times
256×256	12	7.76E-3	3.57E-5	0.43
512×512	12	1.26E-5	2.60E-6	1.62
1024×1024	12	2.50E-6	9.62E-7	7.11
2048×2048	12	2.23E-6	1.49E-7	34.2

solution has second order accuracy in the maximum norm at both interior and exterior grid nodes.

Example 6.4. In this example, we solve the same interface problem with the same exact solution as Example 6.3. The only difference is that the interface is a simply connected curve, given as the zero level set of the smooth function below

$$\Theta(x,y) = (x^2 + y^2) \left(x^2 + y^2 + \frac{1}{2}x \right) - 2xy^2 - \frac{1}{100}.$$

This interface has both positive and negative curvatures. Fig. 7 shows the isolines of a numerical solution to the boundary integral equations (3.10)-(3.11) for the interface prob-

Table 9: Numerical results for the interface problem of Example 6.4 ($\sigma_i=1$ and $\sigma_e=25$).

grid size	#GMRES	$\ e_h\ _{\infty,\Omega_i}$	$\ e_h\ _{\infty,\Omega_e}$	CPU times
256×256	10	3.86E-5	2.92E-5	0.43
512×512	10	8.49E-6	5.56E-6	1.69
1024×1024	10	8.36E-7	7.02E-7	7.73
2048×2048	10	2.17E-7	1.81E-7	36.1

Table 10: Numerical results for the interface problem of Example 6.4 ($\sigma_i=1$ and $\sigma_e=50$).

grid size	#GMRES	$\ e_h\ _{\infty,\Omega_i}$	$\ e_h\ _{\infty,\Omega_e}$	CPU times
256×256	10	3.77E-5	2.85E-5	0.33
512×512	10	8.32E-6	5.41E-6	1.41
1024×1024	10	8.43E-7	7.07E-7	6.13
2048×2048	10	2.41E-7	1.82E-7	29.5

Table 11: Numerical results for the interface problem of Example 6.4 ($\sigma_i=1$ and $\sigma_e=100$).

grid size	#GMRES	$\ e_h\ _{\infty,\Omega_i}$	$\ e_h\ _{\infty,\Omega_e}$	CPU times
256×256	10	3.71E-5	2.81E-5	0.33
512×512	10	8.21E-6	5.34E-6	1.41
1024×1024	10	8.80E-7	7.10E-7	6.16
2048×2048	10	2.94E-7	1.82E-7	29.6

Table 12: Numerical results for the interface problem of Example 6.4 ($\sigma_i=1$ and $\sigma_e=200$).

grid size	#GMRES	$\ e_h\ _{\infty,\Omega_i}$	$\ e_h\ _{\infty,\Omega_e}$	CPU times
256×256	10	3.66E-5	2.79E-5	0.33
512×512	10	8.12E-6	5.30E-6	1.41
1024×1024	10	9.70E-7	7.11E-7	6.15
2048×2048	10	4.01E-7	1.83E-7	29.4

Table 13: Numerical results for the interface problem of Example 6.4 ($\sigma_i=1$ and $\sigma_e=2000$).

grid size	#GMRES	$\ e_h\ _{\infty,\Omega_i}$	$\ e_h\ _{\infty,\Omega_e}$	CPU times
256×256	10	3.17E-5	2.78E-5	0.33
512×512	10	7.08E-6	5.27E-6	1.42
1024×1024	10	2.67E-6	7.13E-7	6.28
2048×2048	10	2.35E-6	1.83E-7	29.7

Table 14: Numerical results for the interface problem of Example 6.4 ($\sigma_i=1$ and $\sigma_e=20000$).

grid size	#GMRES	$\ e_h\ _{\infty,\Omega_i}$	$\ e_h\ _{\infty,\Omega_e}$	CPU times
256×256	10	6.87E-5	2.78E-5	0.34
512×512	10	2.01E-5	5.27E-6	1.42
1024×1024	10	1.97E-5	7.13E-7	6.18
2048×2048	10	2.18E-5	1.83E-7	29.3

lem with the KFBI method. Tables 9-14 have results from solving the BIEs (3.10)-(3.11) for the interface problem with different coefficients. The efficiency and accuracy of the numerical solution observed here are consistent with Example 6.3.

Example 6.5 (Linearized Poisson-Boltzmann Equation). Now we consider a heterogeneous interface problem with piecewise constant coefficients:

$$\sigma_i=1, \quad \kappa_i=0, \quad \sigma_e=4, \quad \text{and} \quad \kappa_e=10.$$

This is the linearized Poisson-Boltzmann equation. It is a heterogeneous interface problem in that the elliptic differential operators on two sides of the interface are of different types.

Table 15: Numerical errors for the interface problem of Example 6.5.

grid size	#GMRES	$\ e_h^{int}\ _\infty$	$\ e_h^{ext}\ _\infty$	CPU times
256×256	12	1.29E-4	8.41E-5	0.40
512×512	12	1.56E-5	1.12E-5	1.59
1024×1024	11	3.80E-6	1.98E-6	6.96
2048×2048	12	3.89E-7	2.73E-7	33.7

The interface Γ for this example is also given by the zero level set of the smooth function

$$\Theta(x,y) = (x^2 + y^2)^2 + ax(x^2 + y^2) - \frac{16}{5}xy^2 + \frac{1}{1000} = 0.$$

Domain Ω is the square, $\Omega = (-1,1) \times (-1,1)$. The charge sources (f_i and f_e) and the interface jumps (g, j) are chosen such that the exact solution to the problem is given by

$$\begin{aligned} u_i(x,y) &= \exp(0.6x + 0.8y) && \text{for } (x,y) \in \Omega_i, \\ u_e(x,y) &= \sin(\pi(x+1)/2) \sin(\pi(y+1)/2) && \text{for } (x,y) \in \Omega_e. \end{aligned}$$

Numerical results for this example are shown in Table 15.

Example 6.6. We consider the interface problem (2.5)-(2.8) with variable coefficients

$$\begin{aligned} \sigma_i(x,y) &= 1 + x^2 + y^2 && \text{in } \Omega_i, \\ \sigma_e(x,y) &= 1.5 + 0.5(\sin(\pi x) + \cos(\pi y)) && \text{in } \Omega_e. \end{aligned}$$

and

$$\begin{aligned} \kappa_i(x,y) &= 1 + \sin(\pi(x+y)) && \text{in } \Omega_i, \\ \kappa_e(x,y) &= x^2 + y^2 && \text{in } \Omega_e \end{aligned}$$

or

$$\kappa_i = 0 \quad \text{in } \Omega_i, \quad \kappa_e = 0 \quad \text{in } \Omega_e.$$

The interface for this example is given as the zero level set of the smooth function

$$\Theta(x,y) = (x^2 + y^2) \left(x^2 + y^2 + \frac{4}{5}x \right) - \frac{16}{5}xy^2 + \frac{1}{1000}.$$

The right hand side (f_i and f_e) and the interface jumps (g and j) are chosen such that the exact solution is the same as the previous example. Numerical results for this example are presented in Tables 16-17. Table 16 corresponds to the case with vanishing reaction coefficients and Table 17 corresponds to the case with non-zero reaction coefficients.

Table 16: Numerical results for the interface problem of Example 6.6 ($\kappa_i = \kappa_e = 0$).

grid size	#GMRES	$\ e_h\ _{\infty, \Omega_i}$	$\ e_h\ _{\infty, \Omega_e}$	CPU times
256×256	12	1.27E-4	1.51E-4	2.53
512×512	12	2.93E-5	3.76E-5	14.3
1024×1024	12	7.35E-6	9.41E-6	64.4
2048×2048	12	1.28E-6	2.35E-6	288.0

Table 17: Numerical results for the interface problem of Example 6.6 ($\kappa_i \neq 0$ and $\kappa_e \neq 0$).

grid size	#GMRES	$\ e_h\ _{\infty, \Omega_i}$	$\ e_h\ _{\infty, \Omega_e}$	CPU times
256×256	12	1.23e-04	1.51e-04	2.02
512×512	12	2.88e-05	3.76e-05	12.6
1024×1024	12	7.23e-06	9.41e-06	63.1
2048×2048	12	1.80e-06	2.35e-06	287.3

Example 6.7. This one also solves the variable coefficients interface problem. It is almost the same as Example 6.6. The only difference is that the interface now is given by the zero level set of the smooth function

$$\Theta(x, y) = (x^2 + y^2) \left(x^2 + y^2 + \frac{1}{2}x \right) - 2xy^2 - \frac{1}{100}.$$

This curve has both positive and negative curvatures. Numerical results for this example are correspondingly presented in Tables 18-19. It happens that the maximum errors for the solution in the exterior domain in this example are the same as those in Example 6.6.

Table 18: Numerical results for the interface problem of Example 6.7 ($\kappa_i = \kappa_e = 0$).

grid size	#GMRES	$\ e_h\ _{\infty, \Omega_i}$	$\ e_h\ _{\infty, \Omega_e}$	CPU times
256×256	12	9.72E-5	1.51E-4	1.94
512×512	12	2.06E-5	3.76E-5	12.7
1024×1024	12	5.06E-6	9.41E-6	63.5
2048×2048	12	1.28E-6	2.35E-6	290.0

Table 19: Numerical results for the interface problem of Example 6.7 ($\kappa_i \neq 0$ and $\kappa_e \neq 0$).

grid size	#GMRES	$\ e_h\ _{\infty, \Omega_i}$	$\ e_h\ _{\infty, \Omega_e}$	CPU times
256×256	12	9.44e-05	1.51e-04	1.90
512×512	12	2.00e-05	3.76e-05	11.8
1024×1024	12	4.92e-06	9.41e-06	58.5
2048×2048	12	1.24e-06	2.35e-06	272.0

The numerical results of Examples 6.5-6.7 all show that the KFBI method for the interface problem yields second-order accurate solutions and the computational work involved is essentially linearly proportional to the number of unknowns.

7 Discussion

This work presents a generalized boundary integral method for the solution of the variable coefficients elliptic partial differential equations, which include both boundary value and interface problems. The method is kernel-free in the sense that there is no need to know analytical expressions for kernels of the boundary (and volume) integrals in the solution of boundary integral equations. With the kernel-free boundary integral method, the evaluation of a boundary or volume integral is replaced by interpolation of a Cartesian grid based solution, which satisfies an equivalent interface problem, while the interface problem on a Cartesian grid is solved by a fast solver. The boundary integral equations for both the boundary value and interface problems solved with the KFBI method are the Fredholm integral equation of the second kind. They are well-conditioned. Numerical experiments verified the well-conditioning of the discrete BIEs, showing that the GMRES iteration numbers used are essentially independent of the grid sizes. The numerical examples show that the numerical solutions by the KFBI method have second-order accuracy.

We have already applied the KFBI method for the variable coefficients boundary value and interface problems in three space dimensions, where we also observed second-order accuracy and optimal efficiency of the method. In three space dimensions, the boundary or surface may be represented by an unstructured (triangle or quadrilateral) grid or the approach proposed in [49].

We remark the methodology for the heterogeneous interface problem in this work is applicable for the general nonlinear Poisson-Boltzmann equation, the Darcy-Stokes equation, etc..

At the moment, one limitation of the KFBI method for variable coefficients elliptic PDEs is that the coefficients $\sigma(\mathbf{p})$ and $\kappa(\mathbf{p})$ are required to have sufficiently smooth extension on $\bar{\mathcal{B}}$. For practical problems, the reaction and diffusion coefficients $\kappa(\mathbf{p})$ and $\sigma(\mathbf{p})$ may have definition only on one side of the interface/boundary Γ . In this case, we first need to extrapolate the coefficients to the other side of Γ so that the coefficients are sufficiently smooth on $\bar{\mathcal{B}}$ before the KFBI method is applied to solve the elliptic PDEs. For the extrapolation, the technique of harmonic or biharmonic extension or others such as the one proposed by Aslam [2] may be used.

Another limitation is that the efficiency of the KFBI method relies on the existence of the Fredholm boundary integral equation of the second kind for the boundary value or interface problem. The well-conditioning of the boundary integral equation guarantees that the number of GMRES iterations is independent of the mesh parameter so that the overall computational work involved is essentially linearly proportional to the number

of grid nodes in the larger rectangle. For some problems of elliptic PDEs, which is impossible or difficult to be reformulated as a well-conditioned integral equation, the KFBI method will lose its efficiency. In this case, the KFBI method may need to be combined with a matrix-free fast direct solver for boundary integral equations.

Acknowledgments

Research of the first author was supported in part by the National Science Foundation of the USA under Grant DMS-0915023, and is supported by the National Natural Science Foundation of China under Grants DMS-11101278 and DMS-91130012. Research of the first author is also supported by the Young Thousand Talents Program of China. Research of the second author is supported in part by National Science Committee of Taiwan under Grant 99-2115-M-007-002-MY2. This work is supported in part by National Center for Theoretical Sciences of Taiwan, too.

Appendix

In this appendix, we present some basic facts about the volume integral, the single layer and double layer boundary integrals associated with the Green function of the variable coefficients elliptic differential operator on the rectangle \mathcal{B} , which embeds the bounded domain Ω and its boundary Γ .

Let

$$\mathcal{A} \equiv \nabla \cdot (\sigma(\mathbf{p}) \nabla) - \kappa(\mathbf{p})$$

be the differential operator. We first have Green's first identity

$$\int_{\Omega} v \mathcal{A} u d\mathbf{q} = \int_{\Gamma} v \mathbf{n} \cdot \sigma \nabla u ds_{\mathbf{q}} - \int_{\Omega} \nabla v \cdot \sigma \nabla u d\mathbf{q} - \int_{\Omega} \kappa u v d\mathbf{q} \quad (\text{A.1})$$

and Green's second identity

$$\int_{\Omega} v \mathcal{A} u d\mathbf{q} - \int_{\Omega} u \mathcal{A} v d\mathbf{q} = \int_{\Gamma} v \mathbf{n} \cdot \sigma \nabla u ds_{\mathbf{q}} - \int_{\Gamma} u \mathbf{n} \cdot \sigma \nabla v ds_{\mathbf{q}} \quad (\text{A.2})$$

for sufficiently smooth functions u and v .

Let $G(\mathbf{q}; \mathbf{p})$ be Green's function of the differential operator \mathcal{A} on \mathcal{B} , which satisfies

$$\begin{aligned} \mathcal{A} G(\mathbf{q}; \mathbf{p}) &= \delta(\mathbf{q} - \mathbf{p}) && \text{in } \mathcal{B}, \\ G(\mathbf{q}; \mathbf{p}) &= 0 && \text{on } \partial \mathcal{B}, \end{aligned}$$

for each fixed $\mathbf{p} \in \mathcal{B}$. The Green function $G(\mathbf{q}; \mathbf{p})$ is symmetric with respect to the independent variables \mathbf{p} and \mathbf{q} , i.e., $G(\mathbf{p}; \mathbf{q}) = G(\mathbf{q}; \mathbf{p})$.

When one of the functions u and v in Green's identities (A.1) and (A.2) is replaced with the Green function $G(\mathbf{q}; \mathbf{p})$, the identities still hold and are called the generalized

Green identities. In particular, the generalized Green first identity implies the Gauss formula

$$\int_{\Gamma} \mathbf{n}_{\mathbf{q}} \cdot \sigma \nabla G(\mathbf{q}; \mathbf{p}) ds_{\mathbf{q}} - \int_{\Omega} \kappa G(\mathbf{q}; \mathbf{p}) d\mathbf{q} = \begin{cases} 1, & \mathbf{p} \in \Omega, \\ \frac{1}{2}, & \mathbf{p} \in \Gamma, \\ 0, & \mathbf{p} \in \Omega^c. \end{cases} \quad (\text{A.3})$$

Here, $\Omega^c = \mathcal{B} \setminus \bar{\Omega}$ is the complement of $\bar{\Omega}$ in \mathcal{B} .

Let $\varphi = \varphi(\mathbf{p})$ and $\psi = \psi(\mathbf{p})$ be two functions defined on Γ and let $f = f(\mathbf{p})$ be a function defined in Ω . Denote by

$$(\mathcal{M}\varphi)(\mathbf{p}) \equiv \int_{\Gamma} \mathbf{n}_{\mathbf{q}} \cdot \sigma(\mathbf{q}) \nabla G(\mathbf{q}; \mathbf{p}) \varphi(\mathbf{q}) ds_{\mathbf{q}}, \quad (\mathcal{L}\psi)(\mathbf{p}) \equiv \int_{\Gamma} G(\mathbf{q}; \mathbf{p}) \psi(\mathbf{q}) ds_{\mathbf{q}}$$

and

$$(\mathcal{G}f)(\mathbf{p}) \equiv \int_{\Omega} G(\mathbf{q}; \mathbf{p}) f(\mathbf{q}) d\mathbf{q}$$

the double layer, single layer boundary and volume integrals, respectively.

In the next, for simplicity, we only introduce three theorems for the case when the density functions f , ψ and φ are continuous or continuously differentiable functions. For general density functions, similar statements can be proved following the lines in Costabel [14] except the Green function there is defined in the free space and needs to be replaced by the current one.

Theorem A.1. *Given a continuous function f defined in Ω , the volume integral $v(\mathbf{p}) = (\mathcal{G}f)(\mathbf{p})$ is continuously differentiable in \mathcal{B} and satisfies the interface problem*

$$\begin{aligned} \mathcal{A}v(\mathbf{p}) &= \begin{cases} f & \text{if } \mathbf{p} \in \Omega, \\ 0 & \text{if } \mathbf{p} \in \Omega^c, \end{cases} \\ [v] &= 0 && \text{on } \Gamma, \\ \sigma[\partial_{\mathbf{n}}v] &= 0 && \text{on } \Gamma, \\ v &= 0 && \text{on } \partial\mathcal{B}. \end{aligned}$$

For a continuous function f defined in Ω^c , the corresponding statement is also true for the volume integral over Ω^c . We omitted the proofs.

The two theorems below are for the single layer and double layer boundary integrals $\mathcal{M}\varphi$ and $\mathcal{L}\psi$. The proof for Theorem A.2 on the single layer boundary integral is similar to but much easier than that for Theorem A.3 on the double layer boundary integral. We only present the proof for the latter one.

Theorem A.2. *For a continuously differentiable function $\psi(\mathbf{p})$ defined on Γ , the single layer potential boundary integral $v(\mathbf{p}) = -\mathcal{L}\psi(\mathbf{p})$ satisfies the interface problem*

$$\begin{aligned} \mathcal{A}v &= \nabla \cdot (\sigma(\mathbf{p}) \nabla v) - \kappa(\mathbf{p})v = 0 && \text{in } \mathcal{B} \setminus \Gamma, \\ [v] &= 0 && \text{on } \Gamma, \\ \sigma[\partial_{\mathbf{n}}v] &= \psi && \text{on } \Gamma, \\ v &= 0 && \text{on } \partial\mathcal{B}. \end{aligned}$$

Moreover, we have the jump relations

$$\begin{aligned} \sigma \partial_{\mathbf{n}} v^+ &= \frac{1}{2} \psi - \sigma \partial_{\mathbf{n}} (\mathcal{L}\psi) && \text{on } \Gamma, \\ \sigma \partial_{\mathbf{n}} v^- &= -\frac{1}{2} \psi - \sigma \partial_{\mathbf{n}} (\mathcal{L}\psi) && \text{on } \Gamma, \end{aligned}$$

where v^+ and v^- are the restrictions of $v(\mathbf{p})$ in the subdomains Ω and Ω^c , respectively.

Let

$$(\mathcal{M}^* \varphi)(\mathbf{p}) \equiv \int_{\Gamma} \mathbf{n}_{\mathbf{p}} \cdot \sigma(\mathbf{p}) \nabla G(\mathbf{q}; \mathbf{p}) \varphi(\mathbf{q}) ds_{\mathbf{q}}, \quad \text{for } \mathbf{p} \in \Gamma$$

be the adjoint double layer boundary integral. The jump relations in Theorem A.2 can be written as

$$\sigma \partial_{\mathbf{n}} v^+ = \frac{1}{2} \psi - \mathcal{M}^* \psi \quad \text{on } \Gamma, \tag{A.4}$$

$$\sigma \partial_{\mathbf{n}} v^- = -\frac{1}{2} \psi - \mathcal{M}^* \psi \quad \text{on } \Gamma, \tag{A.5}$$

since $\sigma \partial_{\mathbf{n}} (\mathcal{L}\psi) = \mathcal{M}^* \psi$.

Theorem A.3. For a continuous function $\varphi(\mathbf{p})$ defined on Γ , the double layer boundary integral $v(\mathbf{p}) = \mathcal{M}\varphi(\mathbf{p})$ satisfies the interface problem

$$\mathcal{A}v \equiv \nabla \cdot (\sigma(\mathbf{p}) \nabla v) - \kappa(\mathbf{p})v = 0 \quad \text{in } \mathcal{B} \setminus \Gamma, \tag{A.6}$$

$$[v] = \varphi \quad \text{on } \Gamma, \tag{A.7}$$

$$\sigma [\partial_{\mathbf{n}} v] = 0 \quad \text{on } \Gamma, \tag{A.8}$$

$$v = 0 \quad \text{on } \partial \mathcal{B}. \tag{A.9}$$

Moreover, we have the jump relations

$$v^+ = \frac{1}{2} \varphi + \mathcal{M}\varphi \quad \text{on } \Gamma, \tag{A.10}$$

$$v^- = -\frac{1}{2} \varphi + \mathcal{M}\varphi \quad \text{on } \Gamma, \tag{A.11}$$

where v^+ and v^- are the restrictions of $v(\mathbf{p})$ in the subdomains Ω and Ω^c , respectively.

In the next, we only prove Theorem A.3 for the case when φ is a smooth function defined on the smooth interface Γ .

Proof. For the double layer potential, we choose a function $w_1(\mathbf{p})$ defined in Ω such that

$$\mathcal{A}w_1 = 0 \quad \text{in } \Omega,$$

$$w_1 = \varphi \quad \text{on } \Gamma.$$

By the generalized Green second identity, we have

$$\begin{aligned}
 (\mathcal{M}\varphi)(\mathbf{p}) &= \int_{\Gamma} (\mathbf{n} \cdot \sigma \nabla G(\mathbf{q}; \mathbf{p})) w_1(\mathbf{q}) ds_{\mathbf{q}} \\
 &= \int_{\Gamma} (\mathbf{n} \cdot \sigma \nabla w_1(\mathbf{q})) G(\mathbf{q}; \mathbf{p}) ds_{\mathbf{q}} + \int_{\Omega} (\mathcal{A}G(\mathbf{q}; \mathbf{p})) w_1(\mathbf{q}) ds_{\mathbf{q}} \\
 &= \int_{\Gamma} (\mathbf{n} \cdot \sigma \nabla w_1(\mathbf{q})) G(\mathbf{q}; \mathbf{p}) ds_{\mathbf{q}} + \begin{cases} w_1(\mathbf{p}) & \text{if } \mathbf{p} \in \Omega, \\ 0 & \text{if } \mathbf{p} \in \Omega^c. \end{cases} \tag{A.12}
 \end{aligned}$$

By the definition of $G(\mathbf{q}; \mathbf{p})$, from (A.12), we see $\mathcal{M}\varphi$ satisfies the boundary condition (A.9). Applying the elliptic operator \mathcal{A} to both sides of (A.12), we get

$$\mathcal{A}(\mathcal{M}\varphi)(\mathbf{p}) = \int_{\Gamma} (\mathbf{n} \cdot \sigma \nabla w_1(\mathbf{q})) \mathcal{A}G(\mathbf{q}; \mathbf{p}) ds_{\mathbf{q}} = 0 \quad \text{in } \mathcal{B} \setminus \Gamma.$$

That is, the double layer boundary integral $\mathcal{M}\varphi$ satisfies the homogeneous PDE (A.6).

In the next, we will show the discontinuity of the function $\mathcal{M}\varphi$ and the continuity of its normal derivative across Γ . Let $w_2(\mathbf{p})$ be the function satisfying the following boundary value problem of the generalized biharmonic equation

$$\begin{aligned}
 \mathcal{A}(\mathcal{A}w_2) &= 0 && \text{in } \Omega, \\
 \mathbf{n} \cdot \sigma \nabla w_2 &= 0 && \text{on } \Gamma, \\
 w_2 &= \varphi && \text{on } \Gamma.
 \end{aligned}$$

Applying the generalized Green second identity to $G(\mathbf{q}, \mathbf{p})$ and $w_2(\mathbf{p})$, we get

$$\begin{aligned}
 &(\mathcal{M}w_2)(\mathbf{p}) - \int_{\Gamma} G(\mathbf{q}, \mathbf{p}) \mathbf{n} \cdot \sigma \nabla w_2 ds_{\mathbf{q}} + (\mathcal{G}\mathcal{A}w_2)(\mathbf{p}) \\
 &= \tilde{w}_2(\mathbf{p}) \equiv \begin{cases} w_2(\mathbf{p}), & \mathbf{p} \in \Omega, \\ \frac{1}{2}w_2(\mathbf{p}), & \mathbf{p} \in \Gamma, \\ 0, & \mathbf{p} \in \Omega^c. \end{cases} \tag{A.13}
 \end{aligned}$$

Here, we extend $w_2(\mathbf{p})$ by zero to Ω^c in the rectangle domain \mathcal{B} and denote the extended function by $\tilde{w}_2(\mathbf{p})$. By the selection of $w_2(\mathbf{p})$, the identity (A.13) can be simplified to be

$$(\mathcal{M}\varphi)(\mathbf{p}) + (\mathcal{G}\mathcal{A}w_2)(\mathbf{p}) = \tilde{w}_2(\mathbf{p}) = \begin{cases} w_2(\mathbf{p}), & \mathbf{p} \in \Omega, \\ \frac{1}{2}w_2(\mathbf{p}), & \mathbf{p} \in \Gamma, \\ 0, & \mathbf{p} \in \Omega^c. \end{cases} \tag{A.14}$$

Note that the volume integral in (A.14), the integral of the product of the Green function G and $\mathcal{A}w_2$, is continuously differentiable in \mathcal{B} , while the normal flux $\mathbf{n} \cdot \sigma \nabla \tilde{w}_2(\mathbf{p})$ of the extended function $\tilde{w}_2(\mathbf{p})$ is continuous across Γ by the construction. From (A.14), we see that double layer potential $\mathcal{M}\varphi$ has the same discontinuity as the extended function $\tilde{w}_2(\mathbf{p})$ across Γ and the normal flux of the double layer potential has the same continuity as the extended function $\tilde{w}_2(\mathbf{p})$. This implies both the first interface condition (A.7) and the second interface condition (A.8) hold. Finally, by the construction of w_2 , the integral identities (A.14) indicate (A.10)-(A.11). □

References

- [1] L. Adams, T. P. Chartier, New geometric immersed interface multigrid solvers, *SIAM J. Sci. Comput.* 25 (2004) 1516–1533.
- [2] T. D. Aslam, A partial differential equation approach to multidimensional extrapolation, *J. Comput. Phys.* 193 (2003) 349–355.
- [3] J. T. Beale, A grid-based boundary integral method for elliptic problems in three-dimensions, *SIAM J. Numer. Anal.* 42 (2004) 599–620.
- [4] J. T. Beale, M. C. Lai, A method for computing nearly singular integrals, *SIAM J. Numer. Anal.* 38 (6) (2001) 1902–1925.
- [5] J. T. Beale, A. T. Layton, On the accuracy of finite difference methods for elliptic problems with interfaces, *Commun. Appl. Math. Comput. Sci.* 1 (2006) 91–119.
- [6] P. A. Berthelsen, A decomposed immersed interface method for variable coefficient elliptic equations with non-smooth and discontinuous solutions, *J. Comput. Phys.* 197 (2004) 364–386.
- [7] J. W. Cahn, J. E. Hilliard, Free energy of a nonuniform system i, *J. Chem. Phys.* 28 (1958) 258–267.
- [8] D. Calhoun, A Cartesian grid method for solving the two-dimensional stream function-vorticity equations in irregular regions, *J. Comput. Phys.* 176 (2002) 231–275.
- [9] T. Chen, J. Strain, Piecewise-polynomial discretization and Krylov-accelerated multigrid for elliptic interface problems, *J. Comput. Phys.* 227 (2008) 7503–7542.
- [10] H. Cheng, J. Huang, T. J. Leiterman, An adaptive fast solver for the modified Helmholtz equation in two space dimensions, *J. Comput. Phys.* 211 (2) (2006) 616–637.
- [11] L. T. Cheng, R. P. Fedkiw, F. Gibou, M. Kang, A second-order accurate symmetric discretization of the Poisson equation on irregular domains, *J. Comput. Phys.* 171 (2001) 205–227.
- [12] I. L. Chern, Y. C. Shu, A coupling interface method for elliptic interface problems, *J. Comput. Phys.* 225 (2007) 2138–2274.
- [13] P. Concus, G. H. Golub, Use of fast direct methods for the efficient numerical solution of nonseparable elliptic equations, *SIAM J. Numer. Anal.* 10 (1973) 1103–1120.
- [14] M. Costabel, Boundary integral operators on Lipschitz domains: Elementary results, *SIAM J. Math. Anal.* 19 (3) (1988) 613–626.
- [15] C. M. Elliott, S. Zheng, On the Cahn-Hilliard equation, *Arch. Rat. Mech. Anal.* 96 (339).
- [16] J. Englund, J. Helsing, A comparison of splittings and integral equation solvers for a non-separable elliptic equation, *BIT Numerical Mathematics* 44 (2004) 675–697.
- [17] A. L. Fogelson, J. P. Keener, Immersed interface methods for Neumann and related problems in two and three dimensions, *SIAM J. Sci. Comput.* 22 (2000) 1630–1654.
- [18] F. Gibou, R. Fedkiw, L.-T. Cheng, M. Kang, A second order accurate symmetric discretization of the Poisson equation on irregular domains, *J. Comput. Phys.* 176 (2002) 205–227.
- [19] C. Henriquez, Simulating the electrical behavior of cardiac tissue using the bidomain model, *Critical Reviews in Biomedical Engineering* 21 (1993) 1–77.
- [20] S. Hou, X.-D. Liu, A numerical method for solving variable coefficient elliptic equation with interfaces, *J. Comput. Phys.* 202 (2005) 411–445.
- [21] B. Huang, B. Tu, B. Lu, A fast direct solver for a class of 3-D elliptic partial differential equation with variable coefficient, *Commun. Comput. Phys.* 12 (2012) 1148–1162.
- [22] J. Huang, L. Greengard, A fast direct solver for elliptic partial differential equations on adaptively refined meshes, *SIAM J. Sci. Comput.* 21 (2000) 1551–1566.
- [23] H. Johansen, P. Colella, A Cartesian grid embedding boundary method for Poisson’s equa-

- tion on irregular domains, *J. Comput. Phys.* 147 (1998) 60–85.
- [24] J. V. Lambers, A multigrid block Krylov subspace spectral method for variable coefficient elliptic PDE, *AIP Conf. Proc.* 1220 (2010) 134–149.
- [25] R. J. LeVeque, Z. Li, The immersed interface method for elliptic equations with discontinuous coefficients and singular sources, *SIAM J. on Num. Anal.* 31 (4) (1994) 1019–1044.
- [26] Z. Li, A fast iterative algorithm for elliptic interface problems, *SIAM J. Numer. Anal.* 35 (1) (1998) 230–254.
- [27] Z. Li, K. Ito, The immersed interface method: numerical solutions of PDEs involving interfaces and irregular domains, *SIAM Frontiers in Applied Mathematics*, 2006.
- [28] Z. L. Li, S. R. Lubkin, Numerical analysis of interfacial two-dimensional Stokes flow with discontinuous viscosity and variable surface tension, *Int. J. Numer. Meth. Fluid.* 37 (2001) 525–540.
- [29] Z. L. Li, W.-C. Wang, I.-L. Chern, M.-C. Lai, New formulations for interface problems in polar coordinates, *SIAM J. Sci. Comput.* 25 (2003) 224–245.
- [30] S. Linge, J. Sundnes, M. Hanslien, G. T. Lines, A. Tveito, Numerical solution of the bidomain equations, *Phil. Trans. R. Soc. A* 367 (2009) 1931–1950.
- [31] X. D. Liu, R. P. Fedkiw, M. Kang, A boundary condition capturing method for Poisson’s equation on irregular domains, *J. Comput. Phys.* 160 (2000) 151–178.
- [32] B. Lu, Y. Zhou, M. Holst, J. McCammon, Recent progress in numerical methods for the Poisson-Boltzmann equation in biophysical applications, *Communications in Computational Physics* 3 (5) (2008) 973–1009.
- [33] A. Mayo, The fast solution of Poisson’s and the biharmonic equations on irregular regions, *SIAM J. Numer. Anal.* 21 (1984) 285–299.
- [34] A. Mayo, Fast high order accurate solution of Laplace’s equation on irregular regions, *SIAM J. Sci. Statist. Comput.* 6 (1985) 144–157.
- [35] C. Min, F. Gibou, H. Ceniceros, A supra-convergent finite difference scheme for the variable coefficient Poisson equation on non-graded grids, *J. Comput. Phys.* 218 (2006) 123.
- [36] M. Oevermann, R. Klein, A Cartesian grid finite volume method for elliptic equations with variable coefficients and embedded interfaces, *J. Comput. Phys.* 219 (2006) 749–769.
- [37] C. S. Peskin, Numerical analysis of blood flow in the heart, *J. Comput. Phys.* 25 (1977) 220–252.
- [38] C. S. Peskin, Lectures on mathematical aspects of physiology, *Lectures in Appl. Math.* 19 (1981) 69–107.
- [39] C. S. Peskin, The immersed boundary method, *Acta Numer.* (2002) 1–39.
- [40] W. Proskurowski, O. Widlund, On the numerical solution of Helmholtz’s equation by the capacitance matrix method, *Math. Comp.* 30 (1976) 433–468.
- [41] B. M. R. P. Fedkiw, T. Aslam, S. Osher, A non-oscillatory Eulerian approach to interfaces in multimaterial flows (the ghost fluid method), *J. Comput. Phys.* 152 (1999) 457–492.
- [42] Y. Saad, *Iterative methods for sparse linear systems*, PWS Publishing Company, Boston, 1996.
- [43] Y. Saad, M. H. Schultz, GMRES: A generalized minimal residual method for solving non-symmetric linear systems, *SIAM J. Sci. Statist. Comput.* 7 (1986) 856–869.
- [44] J. Strain, Fast spectrally-accurate solution of variable-coefficient elliptic problems, *Proc. American Math. Soc.* 122 (3) (1994) 843–850.
- [45] E. J. Vigmond, R. W. dos Santos, A. J. Prassl, M. Deo, G. Plank, Solvers for the cardiac bidomain equations, *Prog. Biophys Mol. Biol.* 96 (2008) 3–18.
- [46] A. Wiegmann, K. P. Bube, The explicit-jump immersed interface method: finite difference

- methods for PDEs with piecewise smooth solutions, *SIAM J. Numer. Anal.* 37 (3) (2000) 827–862.
- [47] W.-J. Ying, J. T. Beale, A fast accurate boundary integral method for potentials on closely packed cells, *Communications in Computational Physics* 14 (4) (2013) 1073–1093.
- [48] W.-J. Ying, C. S. Henriquez, A kernel-free boundary integral method for elliptic boundary value problems, *J. Comp. Phys.* 227 (2) (2007) 1046–1074.
- [49] W.-J. Ying, W.-C. Wang, A kernel-free boundary integral method for implicitly defined surfaces, *Journal of Computational Physics* 252 (2013) 606–624.
- [50] S. Zhou, Z. Wang, B. Li, Mean-field description of ionic size effects with non-uniform ionic sizes: a numerical approach, *Phys. Rev. E* 84 (2011) 021901.
- [51] Y. C. Zhou, S. Zhao, M. Feig, G. W. Wei, High order matched interface and boundary method for elliptic equations with discontinuous coefficients and singular sources, *J. Comput. Phys.* 213 (1) (2006) 1–30.
- [52] J. Zhu, L. Q. Chen, J. Shen, V. Tikare, A. Onuki, Coarsening kinetics from a variable mobility Cahn-Hilliard equation: Application of a semi-implicit Fourier spectral method, *Phys. Rev. E* 60 (1999) 3564.